The Thesis Committee for Marc-Aurèle Chevreau
Certifies that this is the approved version of the following thesis:

New Formulation of Mechanical Specific Energy (MSE) Taking into Account the Hydraulic Effects for PDC Bits

APPROVED BY
SUPERVISING COMMITTEE:

Supervisor:

Kenneth E. Gray

Hugh Daigle

New Formulation of Mechanical Specific Energy (MSE) Taking into Account the Hydraulic Effects for PDC Bits

by

Marc-Aurèle Chevreau

Thesis

Presented to the Faculty of the Graduate School of

The University of Texas at Austin

in Partial Fulfillment

of the Requirements

for the Degree of

Master of Science in Engineering

The University of Texas at Austin

May 2017

Dedication

To my family, my friends from France and from the United States of America who supported me through the process of writing this thesis

Acknowledgements

First, I would like to thank Dr. Kenneth E. Gray for the opportunity he offered me to work with him inside the Winder Windows Industrial Affiliate Program. His expertise was a vital to the realization of this thesis and more widely to my education in the graduate program of the University of Texas at Austin. I would also like to thank Dr. Daigle for reading this thesis and giving me a precious feedback.

Moreover, I would also like to express my gratitude to Wider Windows sponsor companies and their representative. I would especially like to thank Marathon for providing the data used in this thesis.

Finally, all this work would not have been successful without the support of my friends and my family. Among my family, I would like to thank my mother, my siblings but also my grand-parents who believed in me throughout my education. Among my friends, I would also like to recognize my close friends in Austin: Devi, Gregoire and Alexandre and those in France: Clemence, Maialen, Maiwenn, Gladys, Albane, Guillaume, Jean and Thibault.

Abstract

New Formulation of Mechanical Specific Energy (MSE) Taking into Account the Hydraulic Effects for PDC Bits

Marc-Aurèle Chevreau, M.S.E.

The University of Texas at Austin, 2017

Supervisor: Kenneth E. Gray

In today's unstable economic environment, the cost of drilling continues to be the most important limitation factor to drill new wells. Thus, to reach the deepest depth at the lowest price, drilling needs to be optimized. To do so, drillers monitor two values: the rate of penetration (ROP) and the mechanical specific energy (MSE). However, MSE has been proven to be more valuable because it links ROP with drilling parameters as weight on bit (WOB) or torque. Moreover, it allows computation of mechanical efficiency (EFF_M), which is directly linked to the drilling efficiency.

The latest MSE formulations only consist of three components: a thrust one, a rotary one and a hydraulic one, which only represents the action of the jet impacts. The associated mechanical efficiency consists of the minimum MSE (MSE_{min}) divided by the actual MSE. This formulation has been proven to be inaccurate by several authors. In fact, they showed that as hydrostatic pressure increases, the mechanical efficiency decreases.

This decrease has been explained by these authors by the fact that some important hydraulic phenomena are not considered. These phenomena are the shear dilatancy and change in failure mechanism.

Shear dilatancy is the phenomenon that happens when the drill bit shears the rock: the rock dilates which causes a decrease in pore pressure and thus an increase in differential pressure which strengthens the rock. This strengthening has been quantified and MSE has been reformulated to take into account this phenomenon.

At atmospheric conditions, the failure mechanism is usually brittle, creating chip like cutting. However, when applying hydrostatic pressure this failure mode switches towards the ductile mode creating ribbon like cutting. The formulation of the MSE_{min} has been adapted to take into consideration this phenomenon.

In order to help an engineer to take into account these phenomena, a program was developed that shows graphically and quantitatively the influence of these mechanisms. The program allows the user to vary several parameters and is capable of extracting drilling data from an existing Excel sheet. This is important since the influence of these mechanisms can create differences of around 10% between the efficiencies calculated with and without considering these phenomena, and this difference can reach values over 20% in certain formations.

Contents

Table of Figures

Table of Tables

Chapter 1: Introduction

1.1 Motivation

Drilling activity is very expensive. In fact, because of the highly unpredictable environment, drilling can be inefficient and delays can occur. This fact, coupled with the price of renting the technologies involved, can lead to over-budget expenses which cannot be allowed, especially in the current situation of a very low oil price. Thus, since the beginning of hydrocarbon exploitation a lot of resources have been dedicated to make drilling more efficient. The final goal being to reach deeper hydrocarbon reservoirs at lower cost.

Drilling efficiency is principally evaluated by two parameters: the rate of penetration (ROP) and the mechanical specific energy (MSE). The interest of ROP is that it is easy to understand its physical value. It basically represents the velocity at which the bit penetrates the rock. However, the issue of monitoring this value is that it does not easily capture the phenomena happening downhole. For instance, drilling with the same parameters through two rocks with different strength will produce two different ROP; ROP will decrease when drilling the harder rock even if the efficiency of drilling stays the same. On the contrary, MSE, as defined by Teale (1965) is "the work done per volume excavated." The main advantage of MSE over ROP is that it enables linking of ROP with other physical values like torque and weight on bit (WOB). Thus, MSE is able to capture unwanted phenomena like bit-balling, which is very difficult to notice using only ROP. Moreover, in addition to MSE, Teale (1965) introduced a second physical value named the mechanical efficiency (EFF_M), which consists of the minimum MSE (MSE_{min}) divided by the actual MSE. This value is directly related to the bit efficiency and then to the overall drilling efficiency. Thus,

prediction and real time monitoring of MSE are very attractive and effective to optimize drilling.

The motivation for this project is that the current formulations of both MSE and EFF_M have some serious downfalls, especially in the way of accounting for hydraulic effects. First, in the formulation of MSE, the effect of hydraulics is not fully considered. In fact, the two latest formulations of MSE were made by Armenta (2008) and Mohan (2009). In these formulations, MSE is defined as the addition of three components: a thrust and a rotary component, which are supposed to constitute the mechanical work done at the bit, and a third component representing the hydraulic work at the bit. Practically, this term only represents the action of the jet impacts. In addition, the industry when calculating the EFF_M considers that the MSE_{min} is equal to the confined compressive strength (CCS), which is usually calculated in an oversimplified way (that will be presented later) and thus does not fairly represent the strength of the rock in most drilling conditions.

In fact, hydraulics have three other main effects which are not considered into the formulations of MSE and EFF_M. These effects are shear dilatancy, change in failure mechanism and dynamic chip hold down. The purpose of this thesis is to present for each phenomenon a literature review of how it has been previously studied, how to quantify their effects, and finally, including these effects in calculation of MSE or MSE_{min} to define a new EFF_M.

1.2 MSE and EFF_M Modeling in the Literature

The first attempt to define MSE was made by Simon (1963) who introduced the concept of rock drilling energy as "the energy required to break out a unit volume of rock," and which consists of the ratio between "the volume of rock removed per unit time from the bottom of the hole" and "the rate of which work is done by the bit on the rock at the

bottom of the hole." However, the formulation he presented was a bit simplistic since it only took into account the work done by the torque (T):

$$MSE = \frac{8TN}{{D_b}^2 ROP} \tag{1.1}$$

where T is the torque, N is the rotational speed, D_b is the bit diameter and ROP is the rate of penetration.

Teale (1965) gave the final name to this value: the mechanical specific energy (MSE) and reformulated its definition to "the work done per unit volume excavated." In his work, Teale (1965) added a term to represent the work done by the weight on bit (WOB) divided by the bit area (A_b). Thus, the formula proposed by Teale (1965) is composed of two parts: a thrust and a rotary component:

$$MSE = \frac{WOB}{A_b} + \frac{2\pi NT}{A_b ROP} \tag{1.2}$$

A major addition to this way of formulating MSE was done by Pessier (1992), who linked torque and drag through a bit specific coefficient of sliding friction (μ):

$$T = \mu \frac{D_b WOB}{36} \; then \; MSE = WOB * (\frac{1}{A_b} + \frac{13.33\mu N}{D_b ROP}) \tag{1.3}$$

However, it is only in 2008 that the way of formulating MSE was significantly changed. In addition to the previous thrust and rotary components which constitute the mechanical energy develop at the bit, authors began to introduce a new term representing the hydraulic energy. In particular, two authors introduced two new concepts. First, Armenta (2008) presented the drilling specific energy (DSE), which is defined as "the work done to excavate and remove underneath the bit a volume of rock." Then, Mohan (2009) introduced the hydro-mechanical specific energy (HMSE) as the "energy required to drill a volume of rock and remove it from underneath the bit." In practice Mohan (2009) accounted for the action of jet impacts. In both cases, the additional term took the same form, a term proportional to the ratio between HSI_b and the ROP:

$$DSE = \frac{WOB}{A_b} + \frac{120\pi NT}{A_b ROP} - \frac{1.98*10^6*\lambda*HP_b}{A_b ROP} \quad (1.4)$$

$$HMSE = \frac{WOB_e}{A_b} + \frac{120\pi NT}{A_b ROP} + \frac{\eta \Delta P_b Q}{A_b ROP} \quad (1.5)$$

where HP_b is the bit hydraulic power, ΔP_b is the pressure drop across the bit and Q is the flow rate. One can also note the factors (λ and η) used to adjust the weight of this new term. Armenta (2008) called his term the bit hydraulic factor (which is dimensionless), and did not give a mathematical expression to compute it. The only information he gave about this factor is that it decreases when the bit diameter increases, as shown in figure 1.

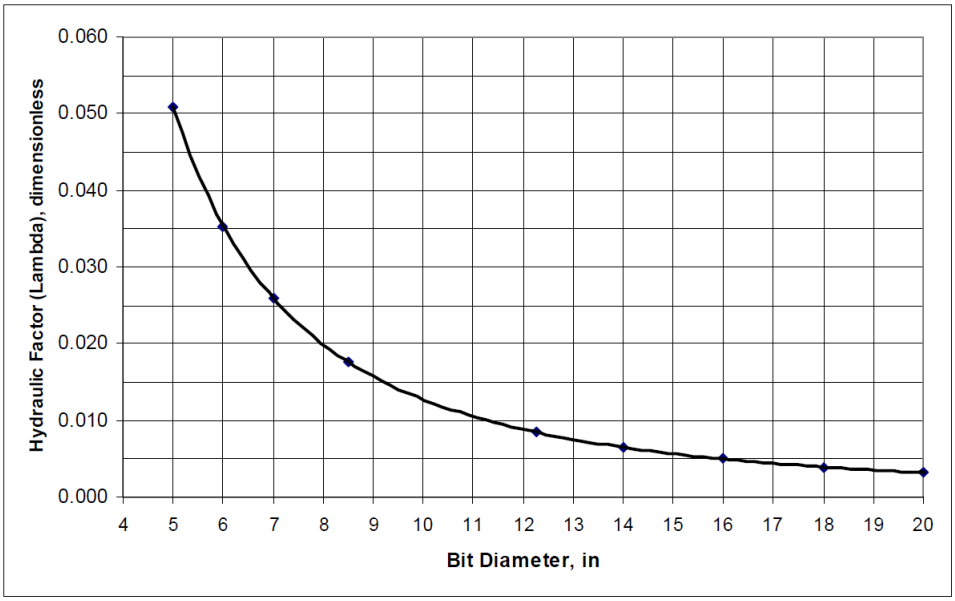

Figure 1 Hydraulic Factor (Lambda) extracted from Armenta (2008)

On the other side, Mohan (2009) gave a very clear and analytical definition of the factor η using the work of Warren (1987) and Rabia (1989) to define the ratio between the energy reaching the formation and the energy available:

$$\eta = \frac{\left(1 - A_v^{-k}\right)}{M^2} \quad (1.6)$$

$$A_v = \frac{0.15*d_b^2}{n*d_n^2} \quad (1.7)$$

$$M = \frac{d_n + 2L * tan(\theta)}{d_n + s * tan(\theta)} \quad (1.8)$$

where n is the number of nozzles, d_n is nozzle diameter, d_b is the bit diameter, L is the length of the potential core, s is the distance of the nozzle from the hole bottom and θ is the angle of axially symmetric jet. In addition to this new term, Mohan (2009) brought another new idea into his paper. It is to consider the pushing force of the jets into the formulation of the thrust component. Thus, he defined an effective weight on bit (WOB_e):

$$WOB_e = WOB - \eta * F_j \quad (1.9)$$

$$F_j = 0.000516 * \rho_m * Q * V_n \quad (1.10)$$

When Teale (1965) first defined the MSE, he stated that a minimum energy exists that is required to crush the rock. This theoretical value for MSE is noted MSE_{min} and depends only on properties of the rock and on the differential pressure between the bottom hole pressure (BHP) and the pore pressure (P_o). This fact is very interesting since the MSE is defined as the addition of the components used to destroy the rock. In fact, in all the formulas this literature contains, the MSE depends only on drilling parameters as the WOB, the torque or the bit hydraulic power. Thus, the MSE as formulated by the authors does not depend on properties of the rock. On the contrary, the MSE_{min} only depends on the parameters of the rock and the bottom hole pressure. However, it has been extensively shown that under some drilling conditions the strength of the rock is modified.

Then, Teale (1965) defined the mechanical efficiency (EFF_M), which is the ratio between the actual MSE and MSE_{min}. In this same paper, he tested this definition at atmospheric condition and found out that the MSE tends towards unconfined compressive strength (UCS) when all the parameters are optimized. Thus, MSE_{min} is assumed to be equal to UCS and drilling is considered efficient when EFF_M reaches 100%.

Pessier (1992) enlarged the tests made by Teale (1965) to hydrostatic conditions. In the case of a borehole pressure varying from 1,000 psi to 5,000 psi, MSE_{min} is guessed to be the confined compressive strength (CCS). However, EFF_M stayed well below 100% even with optimized parameters. In his paper, Pessier (1992) stated that when moving to hydrostatic conditions "there are two phenomena at work: one is the well-known increase in rock strength while under hydrostatic pressure, and the other is the less understood and quantifiable drop in EFF_M."

In practice, Caicedo (2005) showed that the industry takes into account the strengthening of rock due to increase in hydrostatic pressure with a formula like:

$$CCS = UCS + \Delta P * \frac{1+2*\sin(FA)}{1-\sin(FA)} \tag{1.11}$$

where FA is the failure angle, ΔP is the differential pressure between the bottom hole pressure (BHP) and the pore pressure.

In this same paper, the author showed that at deep depths, drilling is considered efficient when the EFF_M reaches only 40%. This fact is the proof that something is wrong in the formulation of MSE and MSE_{min} and was has motivated this thesis.

1.3 Project Description

As said earlier, hydrostatic pressure has two main effects: the strengthening of the rock and the decrease of the mechanical efficiency.

According to Pessier (1992), the phenomenon of strengthening is well known. However, in all the applications found, the failure envelope is considered to be linear. This is surprising since most rocks exhibit a non-linear failure envelope. In fact, as the applied effective stress increases, both the failure angle and the angle of internal friction are changed. In our case the effective stress is the hydrostatic head or the ECD. Since this effect

is said to be “well known”, this thesis will be focused on the second effect of hydrostatic pressure, the decrease of mechanical efficiency.

In fact, this decrease is said to be “less understood and quantifiable”. Since this statement of Pessier (1992), it is only in 2009 that authors began to investigate this phenomenon. In particular, Rafatian (2009) showed that applying the same theory to atmospheric and under pressure rock cutting processes is a misguided practice of the industry. Some of the explanations he proposed to explain this difference between MSE and CCS are shear dilatancy and change in rock failure mode.

In the following paragraphs, the question to know how these mechanisms brought by hydraulics influence drilling and so also influence MSE or MSE_{min} will be answered.

1.3.1 Rock Failure Mechanism

Several articles since 2007 pointed out that the rock failure mechanism actually used in the industry is not accurate in the case of hydrostatic pressure.

Ledgerwood III (2007) showed through particle flow code (PFC) modeling that drillability, which can be measured by the stress difference at high strain, is more influenced by inelastic properties such as the area under the strain curve than elastic properties. In fact, he showed that the energy spent in the cutting process is mainly due to the friction dissipation process in the deformation of rock under pressure. This energy can be up to 50 times larger than the energy spent to break the bonds between grains.

Block (2009) studied the link between the failure mechanism, the cutting structure and the energy spent in the creation of these cuttings using discrete element method (DEM) simulations on polycrystalline diamond compact (PDC) bits. He showed that two main failure modes exist:

- The brittle mode creating chip like cuttings. This mode happens "when the rock is unable to carry load after reaching its peak strength."
- The ductile mode creating ribbon like cuttings due to continuous deformation. This mode happens "when the rock continues to carry load after failure."

Rafatian (2009) showed that the main difference concerning rock cutting processes between atmospheric and under pressure conditions is the cutting mechanism. At atmospheric condition, the cutter must "overcome the bonds between the rock grains" and the intact chip is removed from the rock by the cutter's displacement or the elastic rebound. At under pressure condition, "the shearing of the rock causes a pileup of the crushed rock in front of the cutter." Because of shear dilatancy, the pore pressure in this crushed rock is very low. Thus, there is differential pressure holding this crushed material together. This causes the confining strength of the material to be very high. As the cutter advances, the crushed material is extruded up the face of the cutter. Although the bonds between these grains have been destroyed by the shearing action of the cutter, friction forces between the grains of crushed material are high.

This change of rock failure mechanism is not currently considered in both the MSE and the EFF_M calculations. Since this phenomenon depends only on properties of the rock and on the differential pressure between the BHP and the P_o, it should be considered in the formulation of the MSE_{min}.

1.3.2 Shear Dilatancy

Another phenomenon happening downhole is shear dilatancy. Zijsling (1987) showed that, using a PDC cutter on impermeable rocks, the volumetric expansion due to the shear dilatancy of the rock creates a decrease in pore pressure and thus an increase in differential pressure which strengthens the rock. Ledgerwood III (2007) described the

effect of permeability, “as a drill bit shears rock the rock dilates causing the pore volume to increase. If the rock is impermeable this will cause a reduction of pore pressure increasing differential pressure strengthening the rock.”

However, the works of Judzis (2007) and Black (2008) demonstrate that this strengthening effect is not sufficient to explain the decrease in mechanical efficiency and the rise of MSE when drilling at increasing depth.

This shear dilatancy phenomenon is not currently taken into account in the formulation of MSE or EFF_M. Moreover, since this phenomenon depends both on properties of the rock and on drilling parameters, especially rotational speed, it could be considered in the formulation of MSE or MSE_{min}. The choice made between these two solutions will be discussed later.

1.3.3 The Program

The last goal of this thesis will be to introduce the program used to conducted the studies described above and explain how this program could help drilling engineers to understand when the mechanisms described above have an impact on drilling and how much does this impact weight in the lost or gain of drilling efficiency.

1.4 Thesis Outline

This thesis is composed of five chapters. The first is the introduction and aims to present the project motivation and outline. Each of the next two chapters targets one of the two phenomena previously introduced: the change in failure mechanism and shear dilatancy.

Each phenomenon will be treated as following: first, a literature review will help the reader to understand the phenomenon and how it has been previously studied and

quantified. Then, the way of including this phenomenon into the formulation of MSE and/or EFFM will be discussed. Finally, the newly developed formulation will be tried on real drilling data in order to describe the importance of considering this phenomenon.

Then the fourth chapter will describe the program developed to conduct the previous studies and how to use it.

The last chapter will be the conclusion. It will come back to each phenomenon and on the capacities of the developed program and give ideas on future work.

Chapter 2: Shear Dilatancy

2.1 Literature Review

Shear dilatancy is a major phenomenon happening downhole which happens when the cutter shears the rock. In fact, this shearing causes the rock to dilate. Then, this dilatation decreases pore pressure which increases differential pressure. Finally, this increase in differential pressure strengthens the rock.

Many authors have studied shear dilatancy created by PDC bits. On this topic, some experimental studies have been made using a single PDC cutter facility. The first one was made by Zijsling (1987) followed by Cook (1991) and Gray-Stephens (1994). More recently an extensive set of experimental studies have been conducted on this tool to investigate the effect of pressure on MSE.

However, in this literature review is focused on the analytical studies of shear dilatancy. The first attempt to create a physical model to analyze this phenomenon was made by Detournay (1991) (with an update of his paper in 2000). He took as a starting point the fact that rock strength dependence on pressure is a function of its permeability. In fact, with high-permeability rocks, rock strength is highly dependent on the differential pressure, i.e., the difference between the bottom hole pressure and the pore pressure. However, this fact is not true with low-permeability rocks because of cavitation.

In order to create his model, Detournay (1991) took as a basis for the cutting mechanism the Merchant model (1944, 1945) i.e. the flow mechanism. From this model, Merchant derived some equations:

$$MSE = \frac{2*cos(\varphi)*cos(\vartheta+\psi)}{1-sin(\vartheta+\psi+\varphi)}[c + (p_h - p_o) * tan(\varphi)] \quad (2.1)$$

$$\alpha = \frac{\pi}{4} - \frac{\vartheta+\psi+\varphi}{2} \quad (2.2)$$

$$\vartheta < \frac{\pi}{2} - (\varphi + \psi) \tag{2.3}$$

where ϑ is the rake angle, ψ is the contact friction angle, φ is the internal friction angle, α is the shear failure plane inclination, c is the cohesion, p_h is the bottom hole pressure or in other words the ECD and p_o is the pore pressure in the intact rock. The following figure shows a scheme of the cutting parameters:

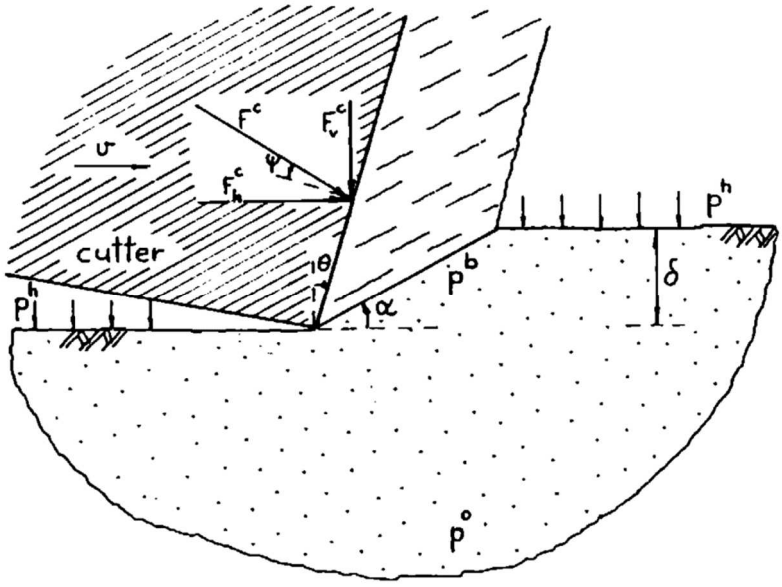

Figure 2 Merchant Failure Mechanism extracted from Detournay (1991)

The main idea of Detournay (1991) is to replace in the Merchant equation the intact pore pressure by the pore pressure along the shear plane. In fact, since these two pressures are different the strength of the rock "seen" by the bit is different from the theoretical "Merchant" strength:

$$MSE = \frac{2*cos(\varphi)*cos(\vartheta+\psi)}{1-sin(\vartheta+\psi+\varphi)}[c + (p_h - p_b) * tan(\varphi)] \tag{2.4}$$

where p_b is the pore pressure along the shear plane. Then the goal is to find a relationship between the pore pressure along the shear plane and the pore pressure in the intact rock.

Detournay (1991) brought two other ideas. Firstly, he stated that $\Delta p = p_b - p_o$ i.e. the difference between the pore pressure along the shear plane (p_b) and the virgin pore pressure (p_o), can be expressed as the product between a function $g(\alpha;\lambda)$ and Δp_* which is the asymptotic value of the pore pressure change for a large λ:

$$\lambda = \frac{v*\delta}{4*c} = \frac{v*\delta*\Phi*C_f*\mu}{4*k} \tag{2.5}$$

where v is the velocity of the cutter, δ is the depth of cut, c is the diffusivity coefficient, Φ is the porosity of the medium, C_f is the compressibility of the fluid, k is the permeability and μ is the dynamic viscosity.

The formula to compute $g(\alpha,\lambda)$ is also given:

$$g(\alpha,\lambda) = \frac{2*i_0(\alpha,\lambda)}{1+i(\alpha,\lambda)} \tag{2.6}$$

$$i(\xi,\alpha,\lambda) = \frac{\sin(\alpha)}{\pi}\int_{-\lambda*\csc(\alpha)}^{\lambda*\csc(\alpha)} e^{(\xi*\lambda*\csc(\alpha)-u)*\cos(\alpha)} K_0(|\xi*\lambda*\csc(\alpha)-u|)du \tag{2.7}$$

$$\xi = \frac{2*s}{l^b} \tag{2.8}$$

Where l^b is the line of length, s is the coordinate along the line, $i_0(\alpha,\lambda)$ is the value of $i(\xi,\alpha,\lambda)$ for $\xi = 0$ and $i(\alpha,\lambda)$ is the average value of $i(\xi,\alpha,\lambda)$ along the line source.

The following image shows a scheme of the different parameters.

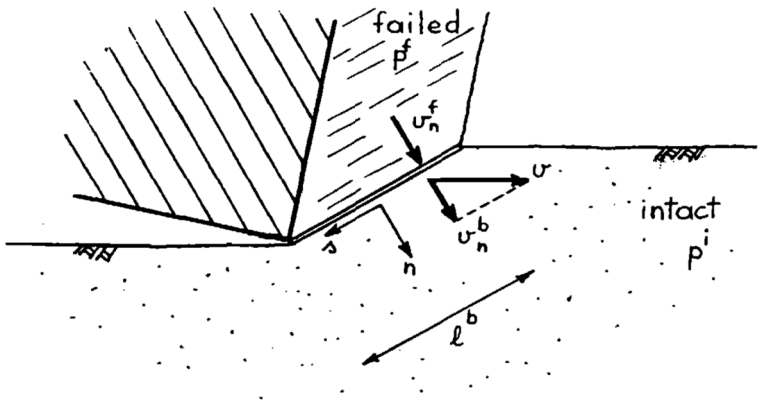

Figure 3 Steadily Moving Velocity Discontinuity Line extracted from Detournay (1991)

Secondly, Detournay (1991) identified three different regimes based on the same dimensionless quantity λ which represent the draining condition.

If $\lambda > 10$, the regime is qualified as "high speed". In this case, the rocks failed on the shear plane in an undrained manner: there is no variation of fluid content in the failed rock. Thus, the drilling response does not depend on the virgin pore pressure. Instead, it is controlled by the variation of pore volume. This leads to very large values of Δp ($= \Delta p_*$), this means that cavitation will happen in the shear zone. Thus $p^b = 0$ and the specific energy only depend on the bottom hole pressure p_h. In fact, the function $g(\alpha; \lambda)$ is equal to 1 which leads to:

$$\Delta p = \Delta p_* = -\frac{\Delta \Phi}{(1-\Phi)} * \frac{\mu * D}{k} = -\frac{\Delta \Phi}{\Phi * (1-\Phi) * C_f} \tag{2.9}$$

$$D = \frac{k}{\Phi * \mu * C_f} \tag{2.10}$$

Where D is the diffusivity coefficient and $\Delta\Phi$ is the pore pressure change.

If $0.001 < \lambda < 10$, the regime is qualified as "transient". In this case, the differential pressure is a function of λ.

$$\Delta p = \Delta p_* * g(\alpha; \lambda) = -\frac{\Delta \Phi}{(1-\Phi)} * \frac{\mu * D}{k} * g(\alpha; \lambda) \tag{2.11}$$

If $\lambda < 0.001$, the regime is qualified as "low speed". In this case the rock responds in a *drained* manner during failure. In this case p_b is determined by the fluid boundary conditions. Then, p_b is in equilibrium with with p_0. In fact, the function $g(\alpha; \lambda)$ is equal to 0 which leads to:

$$\Delta p = 0 \tag{2.12}$$

These results are summarized in the following table:

Value of λ	λ < 0.001	0.001 < λ < 10	λ > 10
Type of Regime	"low speed" =drained	"transient"	"high speed" =undrained
Value of $g(\alpha;\lambda)$	$g(\alpha;\lambda)=0$	$g(\alpha,\lambda)=\frac{2*i_0(\alpha,\lambda)}{1+i(\alpha,\lambda)}$	$g(\alpha;\lambda)=1$
Value of Δp	$\Delta p=0$	$\Delta p=-\frac{\Delta\Phi}{(1-\Phi)}*\frac{\mu*D}{k}*g(\alpha;\lambda)$	p_b=0

Table 1 Summary for Shear Dilatancy

Detournay (2002) also investigated the dependence of MSE on bottom hole pressure in shale. First, the reader needs to recall that shale has a very low permeability and thus is subject to cavitation while drilling. To illustrate his point of view, the author expressed the specific energy as the sum between the specific energy and a term representing the influence of hydraulics:

$$\varepsilon=\varepsilon_0+m*\Delta p\ with\ m=\frac{2*\cos(\varphi)*\cos(\vartheta+\psi)}{1-\sin(\vartheta+\psi+\varphi)} \tag{2.13}$$

$$\Delta p=p_m-p_0 \tag{2.14}$$

However, he discovered that in shale, because of cavitation, the specific energy is only dependent on the bottom hole pressure. Thus, $\varepsilon=\varepsilon_0+m*p_m$. This observation is in concordance with his previous paper. He also came back on the difference between the drained and the undrained case. He stated that the undrained case is highly dependent on hydraulics and, in particular, on the filter cake.

2.2 A New Formulation for MSE

First, the two expressions of MSE has been compared (with and without taking shear dilatancy into account).

$$MSE_{withoutSD} = m * [c + (p_h - p_o) * tan(\varphi)] \quad (2.15)$$

$$MSE_{withSD} = m * [c + (p_h - p_b) * tan(\varphi)] \quad (2.16)$$

$$S = MSE_{withSD} - MSE_{withoutSD} = m[(p_o - p_b) * tan(\varphi)] \quad (2.17)$$

$$S = -m * \Delta p * tan(\varphi) = -m * \Delta p_* * g(\alpha; \lambda) * tan(\varphi) \quad (2.18)$$

$$S = m * \frac{\Delta\Phi}{(1-\Phi)} * \frac{\mu * D}{k} * g(\alpha; \lambda) * tan(\varphi) \quad (2.19)$$

There are two ways of including this Strengthening (S) into the formulation of mechanical efficiency. It depends on either shear dilatancy is considered to be function of properties of the rock and differential pressure between BHP and P_o or a phenomenon controlled by drilling parameters:

- If the shear dilatancy is considered to be only dependent on properties of the rock and differential pressure between BHP and P_o, the strengthening of the rock needs to be included into the formulation of the MSE_{min}:

$$MSE_{min} = CCS + S \quad (2.20)$$

- If the shear dilatancy is considered to be a phenomenon controlled by drilling parameters, the strengthening of the rock needs to be included into the formulation of the MSE:

$$MSE_{withSD} = MSE_{withoutSD} - S \quad (2.21)$$

However, the actual standard of the industry is to compare MSE to CCS to obtain efficiency. Moreover, the strengthening due to shear dilatancy is controlled by the rotational speed or, in other words, by a drilling parameter. Thus, the solution chosen is to consider that shear dilatancy needs to be included in the formulation of the MSE. For clarity

purposes, another physical value was created: the adapted specific energy (ASE) which would be the usual formulation of the MSE minus the strengthening effects not taken into account into the formulation of the MSE.

$$ASE = (work\ done\ to\ destroy\ the\ rock) - (strengthening) \quad (2.22)$$

$$ASE = \left(\frac{WOB}{A_b} + \frac{120\pi NT}{A_b ROP} + \frac{a*HP_b}{A_b ROP}\right) - m * \frac{\Delta\Phi}{(1-\Phi)} * \frac{\mu*D}{k} * g(\alpha;\lambda) * tan(\varphi) \quad (2.23)$$

This value is not the MSE anymore because its final value would be lower than the actual "work done by unit volume removed" (definition by Teale, 1965). However, this value can be compared to the CCS to have a better idea of the real mechanical efficiency.

The reader can also notice that the three different regimes introduced by Detournay (1991) are still applicable with this formulation:

If $\lambda > 10$, "high speed regime" or "undrained regime":

$$ASE = \left(\frac{WOB}{A_b} + \frac{120\pi NT}{A_b ROP} + \frac{a*HP_b}{A_b ROP}\right) - m * \frac{\Delta\Phi}{(1-\Phi)} * \frac{\mu*D}{k} * tan(\varphi) \quad (2.24)$$

If $0.001 < \lambda < 10$, "transient regime":

$$ASE = \left(\frac{WOB}{A_b} + \frac{120\pi NT}{A_b ROP} + \frac{a*HP_b}{A_b ROP}\right) - m * \frac{\Delta\Phi}{(1-\Phi)} * \frac{\mu*D}{k} * g(\alpha;\lambda) * tan(\varphi) \quad (2.25)$$

If $\lambda < 0.001$, "low speed regime" or "drained regime":

$$ASE = \left(\frac{WOB}{A_b} + \frac{120\pi NT}{A_b ROP} + \frac{a*HP_b}{A_b ROP}\right) = MSE \quad (2.26)$$

2.3 Application to Field Data

Much information must be gathered to compute the effect of shear dilatancy. The data used came from Marathon and did not contain all the information needed. Thus, to complete the available information, some assumptions must be made. The following paragraphs will go through the needed physical values and tell if an assumption or data was used.

The first step is to compute λ to know what regime is happening. The formula to compute λ is:

$$\lambda = \frac{v*\delta}{4*c} = \frac{v*\delta*\Phi*C_f*\mu}{4*k} \quad (2.27)$$

Thus, the data needed are:

- The velocity (v): the velocity of cutters is not given but an approximation can be found by multiplying the distance between the center of the bit and the cutter by the rotary speed.
- The depth of cut (δ): the depth of cut is not given but a reasonable approximation is 1 mm = 10^{-3} m.
- The porosity (Φ): The only information contained in Marathon Data on the rock drilled is the formation name, the rock type (sandstone or limestone or shale) and the rock strength. Thus, the porosity (and the permeability (k)) needs to be guessed from the rock type. The assumptions are listed in the following table:

Formation	Porosity	Average Permeability
Sandstone	0.2	100 mD = 10^{-14} m^2
Limestone	0.1	1 mD = 10^{-16} m^2
Shale	0.05	10^{-4} mD = 10^{-22} m^2

Table 2 Formation Assumptions

- The fluid compressibility (C_f): The fluid compressibility is not given. Thus, the fluid compressibility will be set to C_f=5*10^{-4} MPa^{-1}.
- The viscosity of the fluid (μ): The viscosity of the fluid is not given but can be assumed to be equal to 1 cp (=10^{-9} MPa.s).

Thus, the drilling regime (low speed/transient/high speed) will be determined by the rotary speed, the position of the cutter and the nature of the rock.

Since the position of the cutters is needed, some information on the bit geometry must be found. This information will be extracted from the vendor information and common industry practice. The studied section was drilled with a Smith PDC bit, model 616 (6 blades, 16 mm cutters) as indicated by the operator in the BHA report. First, some elements were extracted from the vendor information: the bit diameter (=8.75 in =0.222 m) the number of cutters (50) and the cutter diameter (=0.63 in =0.016 m). Then, using the industry practice, the cutter siderake angle was chosen to be set at 30° (α=30°) and the cutter backrake angle at 10° (θ=10°). However, the most interesting parameter is the radius position of the cutter. The solution found is to divide the bit into five regions then assign a radius to each region and count the number of cutters in each radius. All the interesting values are going to be computed for each radius and then average the strengthening effect using the number of cutters.

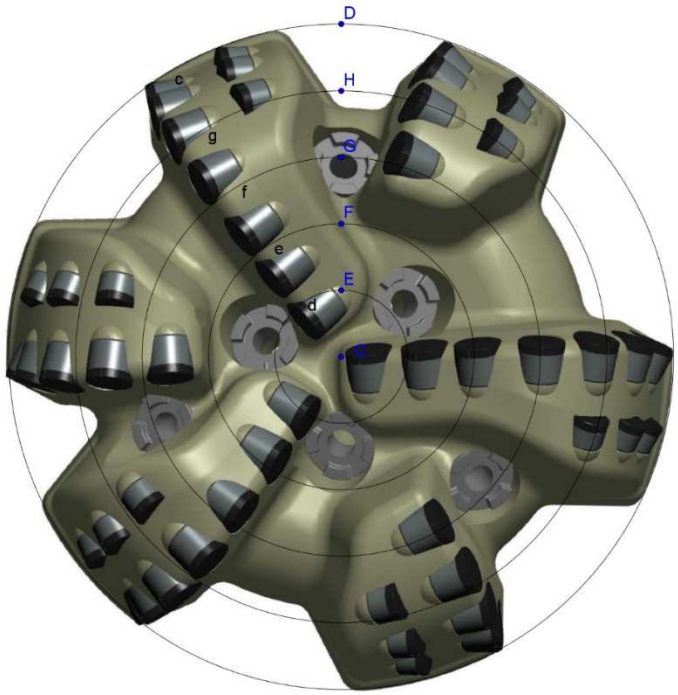

Figure 4 View of a Smith PDC Bit, model 616, extracted from a Schlumberger datasheet

Region	Radius (m)	Number of Cutters
1	0.022225	3
2	0.066675	4
3	0.111125	5
4	0.155575	12
5	0.200025	32

Table 3 Number of Cutter per Radius

This idea of using an average allowed to overcome the first limitation of the model developed by Detournay (1991): the fact that it was conceived for only one cutter.

With these assumptions, the following figure cab be obtained:

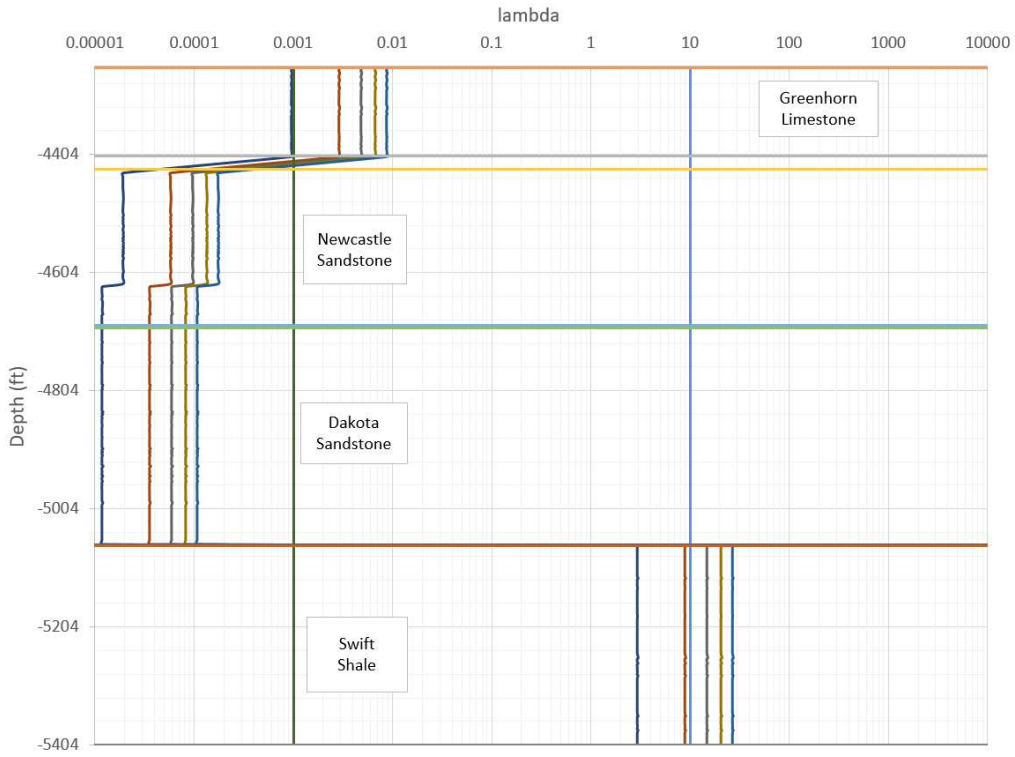

Figure 5 Lambda value for different radii and formations

One the graph above, only the first thousand feet are plotted (for clarity purpose). As one can see on the graph, in the shale the drilling regime is “high speed” for all the radii considered. It can be explained by the fact that shales have a very low permeability and thus cavitation happens systematically in shales. So, shear dilatancy has a strong impact on specific energy.

In the limestone, the drilling regime is “transient” for all the radii considered. So, shear dilatancy will play a role on specific energy. In the sandstones, the smaller radii behave in the “low speed” regime, in the larger radii behave in the “transient” regime. Thus, in the sandstones, shear dilatancy will probably have a negligible impact.

However, in all the rocks considered some radii behave in either the “high speed” regime or the “transient” regime. This means that shear dilatancy has a direct impact on MSE and that ASE needs to be used instead of MSE (or HMSE) to compute mechanical efficiency.

Then, ASE needs to be computed. To do so, some other physical values are needed:

$$S = m * \frac{\Delta\Phi}{\Phi*(1-\Phi)*C_f} * g(\vartheta;\lambda) * tan(\varphi) \tag{2.28}$$

$$m = \frac{2*cos(\varphi)*cos(\vartheta+\psi)}{1-sin(\vartheta+\psi+\varphi)} \tag{2.29}$$

- The assumptions on porosity, fluid compressibility, siderake angle are the same as previously.
- The external friction angle (φ) is assumed to be 60 degrees.
- The external friction angle is assumed to be proportional to internal friction angle (ψ): $\psi = \frac{2}{3}\varphi$. This assumption is commonly made by Miedema (2012).

- The variation of porosity ($\Delta\Phi$) is assumed to be proportional to porosity (Φ): $\Delta\Phi = 0.1 * \Phi$. This assumption is used by Detournay (1991) himself in the example he gave in the paper presented earlier.
- The last interesting feature is the function $g(\vartheta;\lambda)$:
  - If $\lambda > 10$ then $g(\vartheta;\lambda) = 1$ and the regime is "high speed."
  - If $\lambda < 0.001$ then $g(\vartheta;\lambda) = 0$ and the regime is "low speed."
  - If $0.001 < \lambda < 10$ then the regime is "high speed" and $g(\vartheta;\lambda)$ is difficult to determine. Thus, some simplifications will be used:
    - When $\lambda < 0.01$,

$$g(\vartheta;\lambda) = -\frac{4\lambda}{\pi}\ln\left(\frac{\lambda}{sin(\vartheta)}\right) \tag{2.30}$$

    - The next step is to use an Hermite element: This element allows fit a curve by specifying a value for the function and its derivative at each boundary, in this case 0.01 and 1. The use of this element allows to simplify the formulation of $g(\vartheta;\lambda)$.

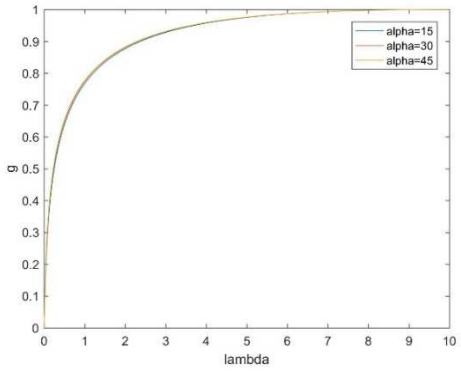

Figure 6 Function g versus Lambda for Different Blade Angles

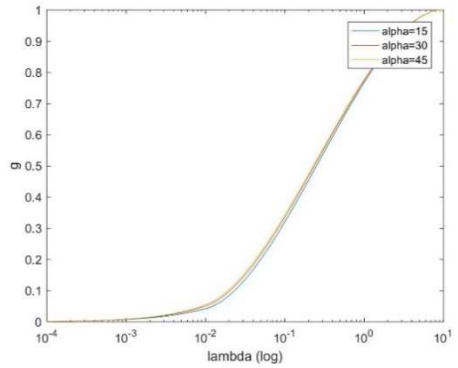

Figure 7 Function g versus log(Lambda) for Different Blade Angles

- The real g function is shown below

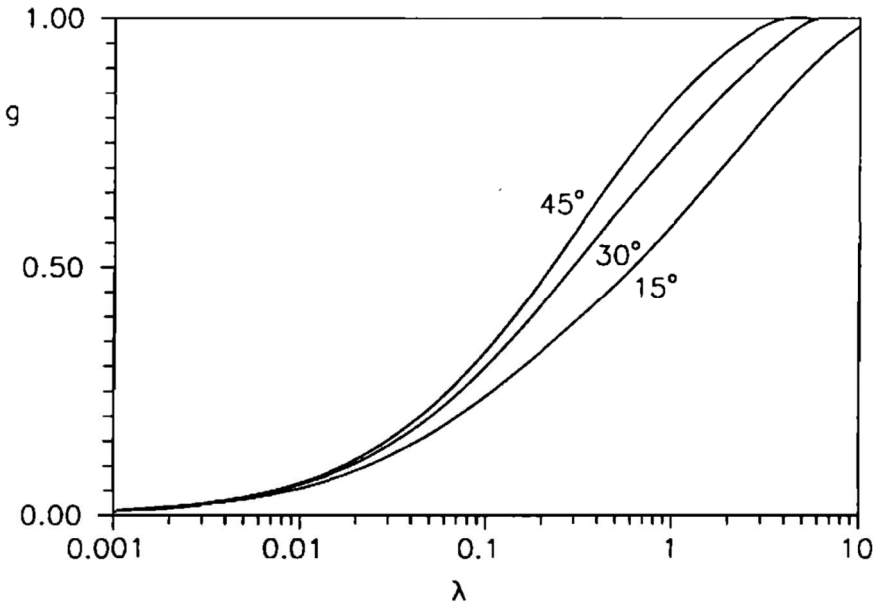

Figure 8 Function g versus log(Lambda) for Different Blade Angles extracted from Detournay (1991)

The second limitation to overcome is the fact that the model developed by Detournay (1991) is a 2D model. However, obviously, the real cutting process is in 3D. Thus, in addition to the backrake angle, the siderake angle should play a role.

This limitation was overcome using the work of Melo (2014) who published a 3D version of the formula developed by Merchant. Using this latest version m becomes:

$$m = \frac{cos(\alpha_S)*(cos(\theta+\psi_n)+tan(\beta)*tan(\psi_s))}{sin(\alpha_n)*(cos(\alpha_n+\theta+\psi_n)-k*cos(\alpha_S)*sin(\alpha_n+\theta+\psi_n))} \quad (2.31)$$

Moreover, the author gave the following relations:

Symbol	Name	Relation
α_S	Lateral angle of failure	$\alpha_S = 0$
α_n	Normal angle of failure	$\alpha_n = \frac{180}{4} - \frac{\psi_n + \varphi + \theta}{2}$
ψ_s	Lateral angle of friction	$\psi_S = 1.2 * \beta$
ψ_n	Normal angle of friction	$\psi_n = 35 - 0.8 * \theta$
θ	Backrake angle	
β	Siderake angle	
φ	Internal friction angle	
k	Mohr Coulomb friction coefficient	$k = \tan(\varphi)$

Table 4 Definition of 3D Parameters

Using this formula, one can obtain the following graph which shows the influence of the siderake angle:

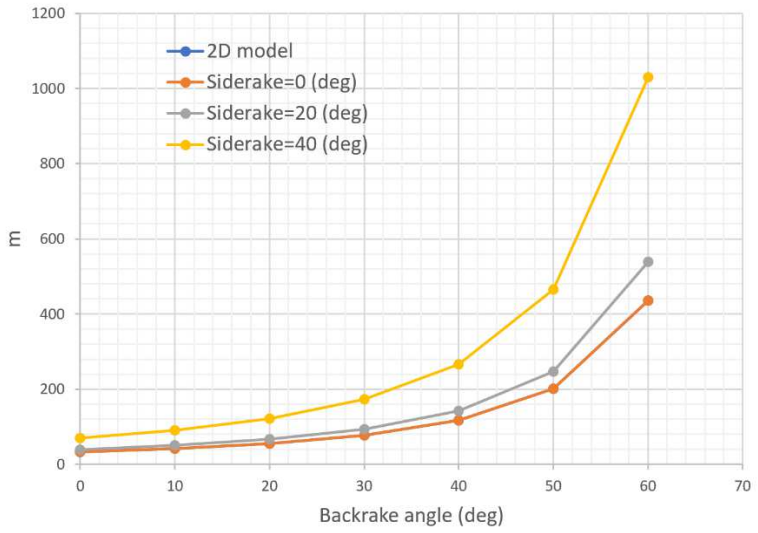

Figure 9 Plot of m versus the Backrake Angle for Different Siderake Angles

As one can easily see on the graph the MSE would be really underestimated using a 2D model.

Using these assumptions, the strengthening can be computed for each radius and then averaging using the number of cutters.

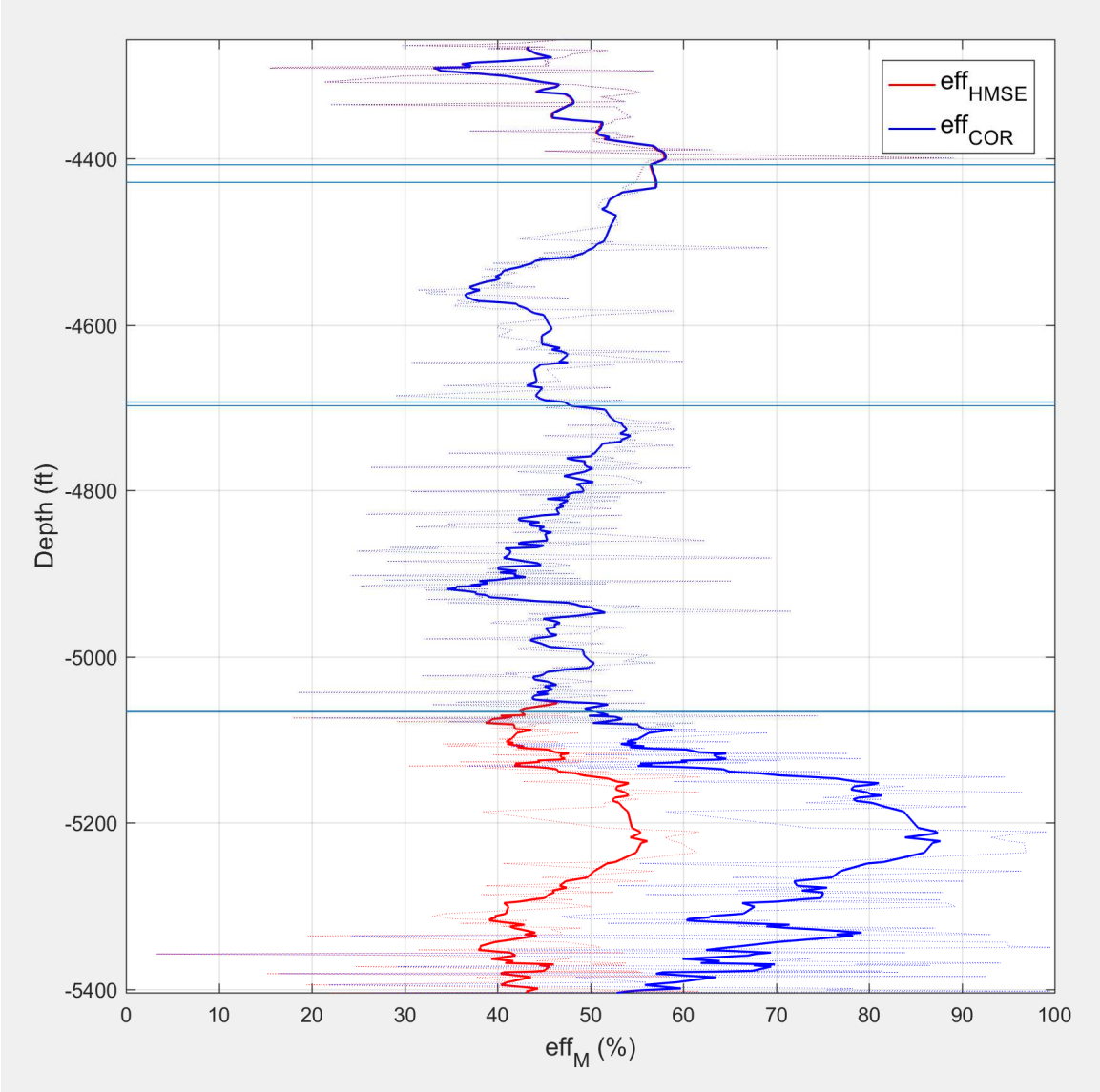

Figure 10 Influence of Shear Dilatancy for the First Four Formations

One the graph above, only the first thousand feet are plotted (for clarity purpose) and the horizontal lines are used to separate the different formations. As one can see on the

previous graph the two lines can be distinguished. The red line is the mechanical efficiency without considering shear dilatancy and the blue line is the mechanical efficiency with considering shear dilatancy.

The following table contains the average mechanical efficiency calculated with HMSE and MSE and the difference between the two for each formation.

Rock Layer	**Eff_M (MSE) (%)**	**Eff_M (ASE) (%)**	**Average Difference (%)**
Greenhorn Limestone	46.22	46.33	0.12
Newcastle Sandstone	44.39	44.39	0.00
Dakota Sandstone	45.95	45.95	0.00
Swift Shale	45.03	66.91	21.88

Table 5 Influence of Shear Dilatancy per Formation for the First Four Formations

As the table shows, shear dilatancy can be neglected in sandstones but it plays a strong role in the shale. The limestone case is particular since the effect of shear dilatancy is not strong but is not negligible either.

2.4 Global Results

The global results are shown below. The point with an efficiency below 0% or above 100% are suppressed. The number of points suppressed are summarized in the following table. The results will be considered as trustworthy if the percentage of the number of points suppressed is under 5%.

Number of Points Suppressed	75
Number of Points Suppressed (%)	1.01

Table 6 Number of Points Suppressed

Rock Type	Eff_M (MSE) (%)	Eff_M (ASE) (%)	Average Difference (%)
Sandstone	25.28	25.28	0.00
Limestone	24.96	24.97	0.01
Shale	25.13	32.65	7.52

Table 7 In fluence of Shear Dilatancy for each Rock Type

On the table above the efficiencies are averaged on the type of rock. As one can see, in the sandstone, the average difference is negligible (approximately 0). For the Limestone, the difference is also negligible but still larger than the sandstone. Finally, for the shale, the averaged difference is 7.52% but as the table below shows, (which described the previous values for each formation) this average difference can reach 21.88% in the Swift shale.

Formation Name	Eff_M (MSE) (%)	Eff_M (ASE) (%)	Average Difference (%)
Greenhorn	46.22	46.33	0.12
Newcastle	44.39	44.39	0.00
Dakota	45.95	45.95	0.00
Swift	45.03	66.91	21.88
Rierdon	35.81	35.85	0.03
Piper	32.18	32.20	0.02
Spearfish	36.44	36.44	0.00
Pine Salt	26.92	26.92	0.00
Broom Creek	21.20	21.20	0.00
Tyler	20.59	20.59	0.00
Kibbey Lime	19.83	21.93	2.10
Charles	22.82	22.82	0.01
Ratcliffe	24.83	24.83	0.00
Base Last Salt	20.48	20.48	0.00
Mission Canyon	23.61	23.62	0.01
Lodgepole	21.24	21.25	0.00

Table 8 In fluence of Shear Dilatancy for each Formation

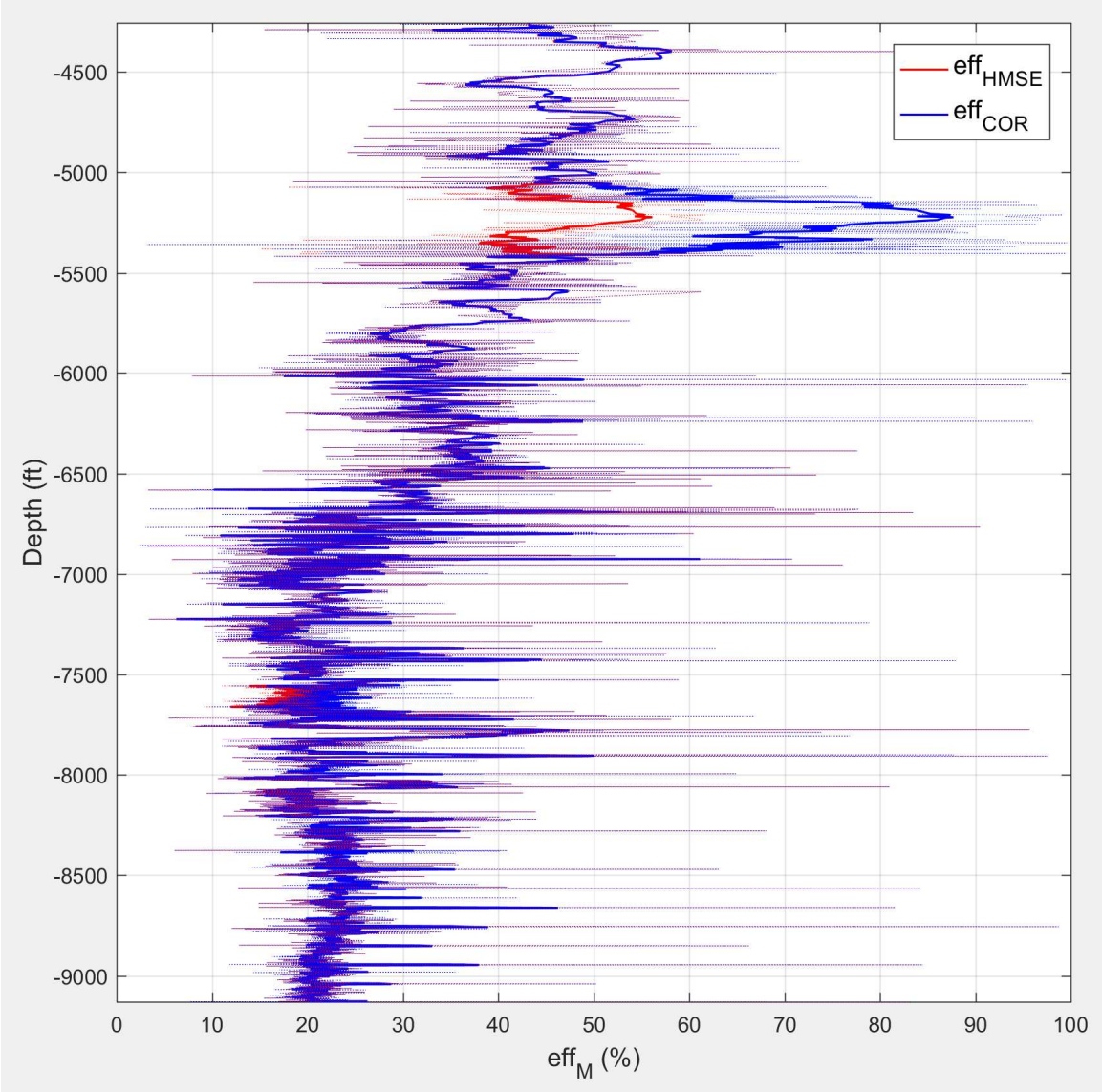

Figure 11 Influence of Shear Dilatancy for the Entire Section

2.5 Parameter Study

2.5.1 Cutter Depth (δ)

If the cutter depth increases from 0.1 mm to 10 cm. The results are presented as following with:

Formation Name	Average Difference (%)			
	δ=0.1mm	δ=1mm	δ=10mm	δ=100mm
Greenhorn	0.00	0.12	0.86	2.59
Newcastle	0.00	0.00	0.03	0.18
Dakota	0.00	0.00	0.01	0.14
Swift	2.76	21.88	23.11	23.11
Rierdon	0.00	0.03	0.25	0.88
Piper	0.00	0.02	0.13	0.47
Spearfish	0.00	0.00	0.01	0.05
Pine Salt	0.00	0.00	0.00	0.03
Broom Creek	0.00	0.00	0.00	0.02
Tyler	0.00	0.00	0.00	0.02
Kibbey Lime	0.14	2.10	2.43	2.46
Charles	0.00	0.01	0.04	0.13
Ratcliffe	0.00	0.00	0.00	0.02
Base Last Salt	0.00	0.00	0.02	0.08
Mission Canyon	0.00	0.01	0.04	0.15
Lodgepole	0.00	0.00	0.03	0.12

Table 9 Influence of Cutter Depth on Shear Dilatancy

As the reader can see, the difference between the EFF_M computed with and without using shear dilatancy increases when the cutter depth increases.

2.5.2 Porosity (Φ)

The porosity has been set for each rock type to the following values (in percent) 0.1, 10, 20, 30 and 40 without changing the permeability

Rock Type	**Average Difference (%)**				
	Φ=0.1%	**Φ=10%**	**Φ=20%**	**Φ=30%**	**Φ=40%**
Sandstone	0.00	0.00	0.00	0.00	0.00
Limestone	0.00	0.01	0.02	0.03	0.05
Shale	0.61	7.45	7.65	7.68	7.68

Table 10 Influence of Porosity on Shear Dilatancy

As one can see on the table, as the porosity increases the average difference increases too. However, the average difference is still very low in the sandstones and in the limestones.

2.5.3 Permeability (k)

The permeability has been multiplied for each rock type to the following values 10^{-2}, 10^{-1}, 10^{0}, 10^{1} and 10^{2} without changing the porosity.

Rock Type	**Average Difference (%)**				
	k/100	**k/10**	**k**	**k*10**	**k*100**
Sandstone	0.03	0.00	0.00	0.00	0.00
Limestone	0.27	0.08	0.01	0.00	0.00
Shale	7.68	7.68	7.52	0.97	0.48

Table 11 Influence of Permeability on Shear Dilatancy

As one can see on the table, as the permeability decreases the average difference increases. However, the average difference is still very low in the sandstones and in the limestones.

2.5.4 Porosity Change ($\Delta\Phi$)

The porosity change was previously assumed to be equal to the porosity multiplied by 0.1. For this study, this multiplication factor will be set to 0.01, 0.1, 0.2, 0.5 and 1.

Formation Name	Average Difference (%)				
	0.01	**0.1**	**0.2**	**0.5**	**1**
Greenhorn	0.01	0.12	0.24	0.60	1.21
Newcastle	0.00	0.00	0.00	0.00	0.00
Dakota	0.00	0.00	0.00	0.00	0.00
Swift	21.91	21.88	21.99	22.58	22.94
Rierdon	0.00	0.03	0.07	0.17	0.35
Piper	0.00	0.02	0.04	0.09	0.19
Spearfish	0.00	0.00	0.00	0.00	0.00
Pine Salt	0.00	0.00	0.00	0.00	0.00
Broom Creek	0.00	0.00	0.00	0.00	0.00
Tyler	0.00	0.00	0.00	0.00	0.00
Kibbey Lime	2.08	2.10	2.13	2.20	2.34
Charles	0.00	0.01	0.01	0.03	0.05
Ratcliffe	0.00	0.00	0.00	0.00	0.00
Base Last Salt	0.00	0.00	0.01	0.01	0.03
Mission Canyon	0.00	0.01	0.01	0.03	0.06
Lodgepole	0.00	0.00	0.01	0.02	0.05

Table 12 Influence of Porosity Change on Shear Dilatancy

The average difference between the efficiency computed HMSE and ASE increases when the porosity change increases.

2.5.5 Influence of 1D, 2D and 3D Use

In order to compute MSE_{min} and the strengthening, one need to use a multiplication factor "m":

$$CCS = UCS + m * \Delta p \tag{2.32}$$

$$S = m * \frac{\Delta \Phi}{\Phi * (1-\Phi) * C_f} * g(\alpha; \lambda) * tan(\varphi) \tag{2.33}$$

$$m_{1D} = 2 * \frac{\sin(FA)}{1-\sin(FA)} \tag{2.34}$$

$$m_{2D} = \frac{2 * cos(\varphi) * cos(\vartheta + \psi)}{1 - sin(\vartheta + \psi + \varphi)} \tag{2.35}$$

$$m_{3D} = \frac{cos(\alpha_S) * (cos(\theta + \psi_n) + tan(\beta) * tan(\psi_s))}{sin(\alpha_n) * (cos(\alpha_n + \theta + \psi_n) - k * cos(\alpha_S) * sin(\alpha_n + \theta + \psi_n))} \tag{2.36}$$

Since the formulation of the strengthening due to shear dilatancy has been defined in this thesis, it will consider that for ASE formulation, the multiplication factor considered will not be changed (this multiplication factor is the 3D one).

On the contrary, CCS can be calculated with the three formulations. The following graph are made using these three multiplication factors: the first using m_{1D}, the second one m_{2D}, and the last one m_{3D}. It should be noticed that the previous studies have been made with m_{3D}.

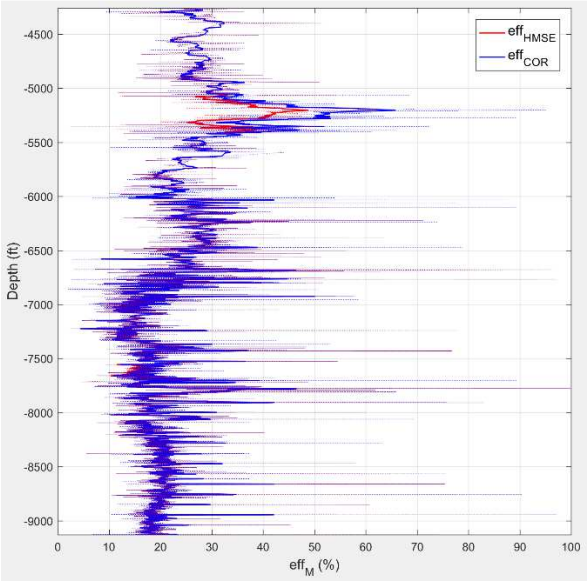

Figure 12 Plot of Efficiency Using 1D to compute CCS

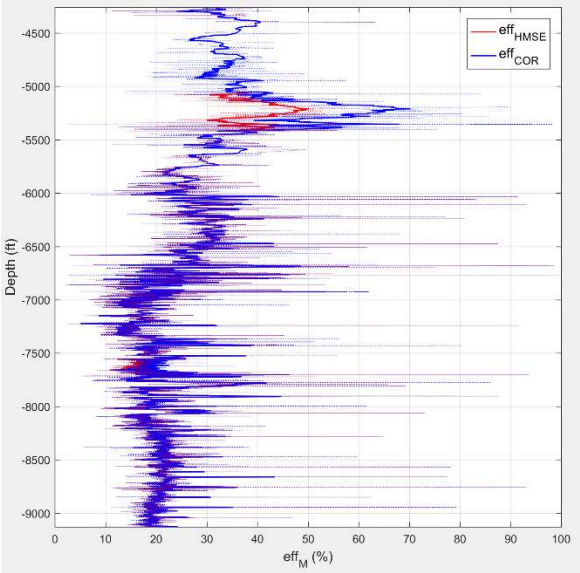

Figure 13 Plot of Efficiency Using 2D to compute CCS

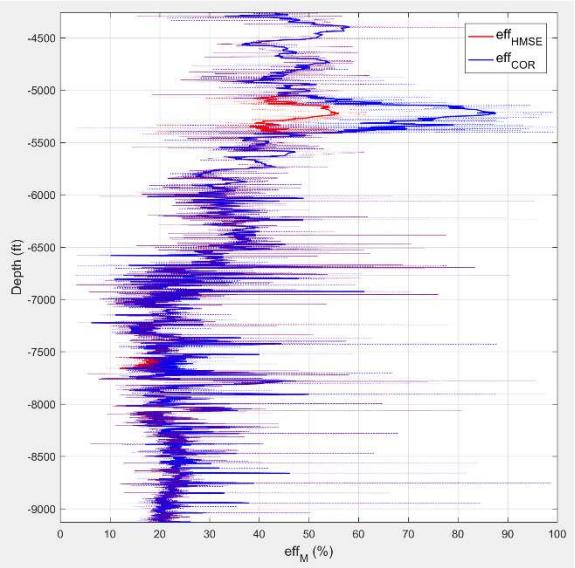

Figure 14 Plot of Efficiency Using 3D to compute CCS

As one can see, the efficiency increases when the number of dimensions increases: for example, in the sandstone layers the efficiency computed with ASE increases from 20.29% in 1D to 21.89% in 2D and finally 25.28% in 3D. The following graph, compare the efficiency computed with HMSE using 1D for CCS and the efficiency computed with ASE using 3D for CCS. In other words, the following graph compare the formulation of MSE developed in this thesis with the formulation currently used by the industry.

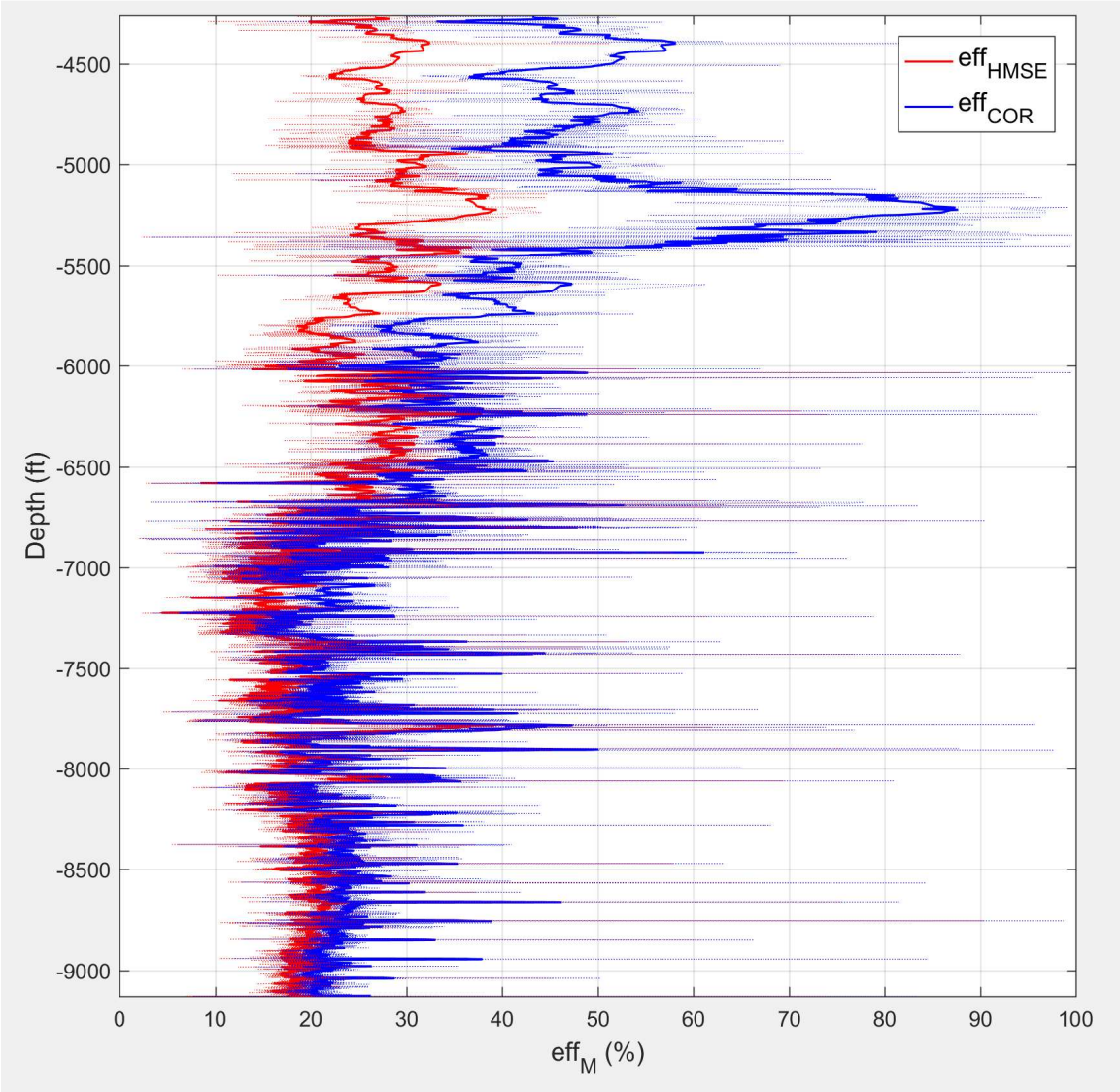

Figure 15 Influence of Shear Dilatancy and 3D Model Combined

Rock Type	EFF_M (HMSE) (%)	EFF_M (ASE) (%)	Average Difference (%)
Sandstone	20.16	25.28	5.12
Limestone	20.98	24.97	3.99
Shale	19.78	32.65	12.87

Table 13 Influence of Shear Dilatancy and 3D

2.6 Conclusion

The effect of shear dilatancy has been quantified and formulated to be included into the formulation of MSE. This led to creation of a new physical value called ASE (Adapted Specific Energy). As it has been shown in the parameter study, the cutter depth, the porosity and the porosity change have very little effect on shear dilatancy, except at very extreme values. On the contrary, permeability has a very strong effect on this phenomenon as low permeability create cavitation. As a reminder, cavitation happens in shale due to the natural low permeability according to Detournay (2000). It can also happen for example in tight gas sandstone and limestone due to low permeability. The following figure shows the extreme case on which the well would be drilled with complete cavitation shear dilatancy becomes predominant. Another important phenomenon is the choice made to consider 1D, 2D or 3D.

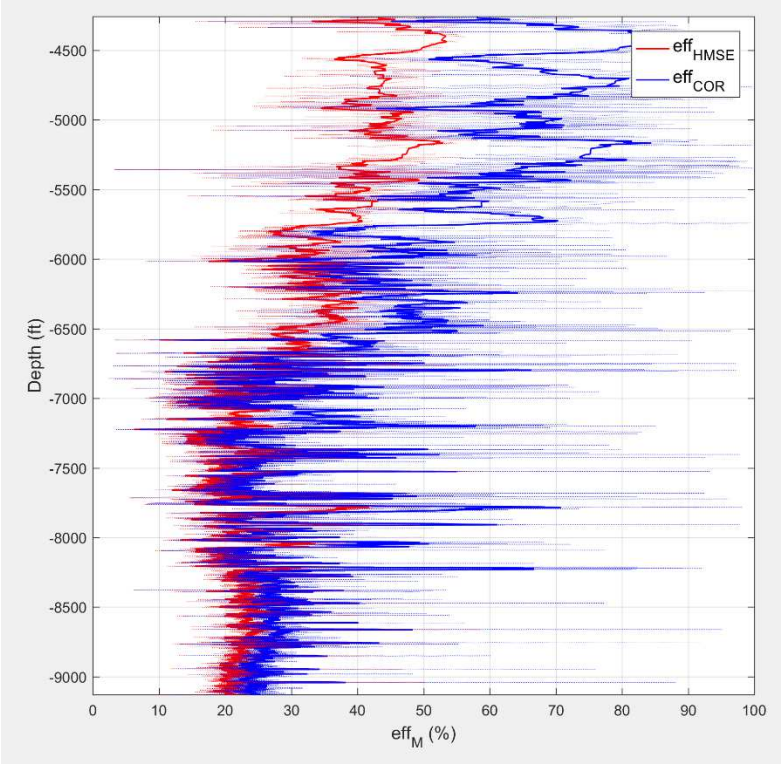

Figure 16 Extreme Case of Cavitation Throughout the Section

Chapter 3: Rock Cutting Mechanism

3.1 Literature Review

Several articles since 2007 point out that the rock failure mechanism currently used in the industry is not accurate in the case of hydrostatic pressure. In particular, three articles by Ledgerwood III (2007), Block (2009) and Rafatian (2009) show the change of failure mechanism from ductile to brittle while increasing the hydrostatic pressure as described in chapter 1.

These authors noticed the change in cutting geometry when increasing hydrostatic pressure. In fact, at low hydrostatic pressure, the cutting process creates chip-like cuttings due to the cutting mode being brittle. On the contrary at high hydrostatic pressure, the cutting mode becomes ductile, creating ribbon-like cuttings.

All of this work to formulate and quantify this change of cutting mechanism is based on work by Miedema (2012). This paper reviews some of the models used to simulate rock cutting for a single PDC cutter. This thesis will focus on the models used to describe the cutting mechanisms for atmospheric conditions and try to adapt these models to hydrostatic conditions.

The authors start by describing the model created by Merchant for steel cutting. From this model, the author will create and describe the different modes and types of failure.

3.1.1 Merchant Model

The model described by Merchant in 1944 and 1945 relies on two assumptions: the deformation is plastic and the chip formation is continuous. This corresponds to a ductile

failure. The formula he developed described the horizontal and vertical forces (respectively F_h and F_v) as follows:

$$F_h = \frac{2*c*h_i*w*\cos(\varphi)*\sin(\alpha+\delta)}{1+\cos(\alpha+\delta+\varphi)} = \lambda_{HF} * c * h_i * w \tag{3.1}$$

$$\lambda_{HF} = \frac{2*\cos(\varphi)*\sin(\alpha+\delta)}{1+\cos(\alpha+\delta+\varphi)} \tag{3.2}$$

$$F_v = \frac{2*c*h_i*w*\cos(\varphi)*\cos(\alpha+\delta)}{1+\cos(\alpha+\delta+\varphi)} = \lambda_{VF} * c * h_i * w \tag{3.3}$$

$$\lambda_{VF} = \frac{2*\cos(\varphi)*\cos(\alpha+\delta)}{1+\cos(\alpha+\delta+\varphi)} \tag{3.4}$$

where c is the cohesive shear strength (=τ_c), h_i is the thickness of the layer cut, w is the width of the cutter, φ is the internal friction angle, α is the blade angle, and δ is the external friction angle. Moreover, it can be noticed that $c = \frac{UCS}{2} * \left(\frac{1-\sin(\varphi)}{\cos(\varphi)}\right)$ where UCS is the unconfined compressive strength. Using this model, the formula for mechanical specific energy (MSE) becomes:

$$MSE = \frac{F_h}{h_i*w} = \lambda_{HF} * c = \frac{\cos(\varphi)*\sin(\alpha+\delta)*UCS}{1+\cos(\alpha+\delta+\varphi)} * \left(\frac{1-\sin(\varphi)}{\cos(\varphi)}\right) \tag{3.5}$$

The goal of Miedema (2012) has been to adapt this model to different failure modes.

3.1.2 The Different Types and Modes of Failure

Thee different types of failure exist. The failure can be brittle, brittle-ductile or completely ductile. Moreover, the failure can also be tensile, shear or a combination of both. Thus, combining each type of failure with each failure mode, nine possibilities can be obtained.

The different types of failure are determined by the rock properties, in particular the ductility number (Dn) which can be defined as the ratio between the unconfined compressive strength and the Brazilian tensile strength, (UCS/BTS) (Miedema, 2015). This

Brazilian tensile strength (BTS) is not the tensile strength value but instead the circle for tensile strength. It accounts for the range of UCS/BTS as relates to brittle, ductile and transitional behavior in the family of circles covering same behaviors.

In fact, the ductility number allows for separating brittle, brittle-ductile and ductile failure. Gehring (1987) stated that pseudo-ductile failure happens when D_n is below 9, brittle failure happens when D_n is larger than 15 and brittle-ductile happens when D_n is between 9 and 15. The term "pseudo-ductile" is due to the fact that the mechanism "shows a ductile behavior in the stress-strain curve […] but it is destructive and not plastic" (Miedema, 2015). As showed, in the followed picture, the ductile failure is a continuous process whereas the brittle failure is a discontinues mechanism: the force builds up then when the rock reaches its limit the rock breaks and the force decreases very rapidly.

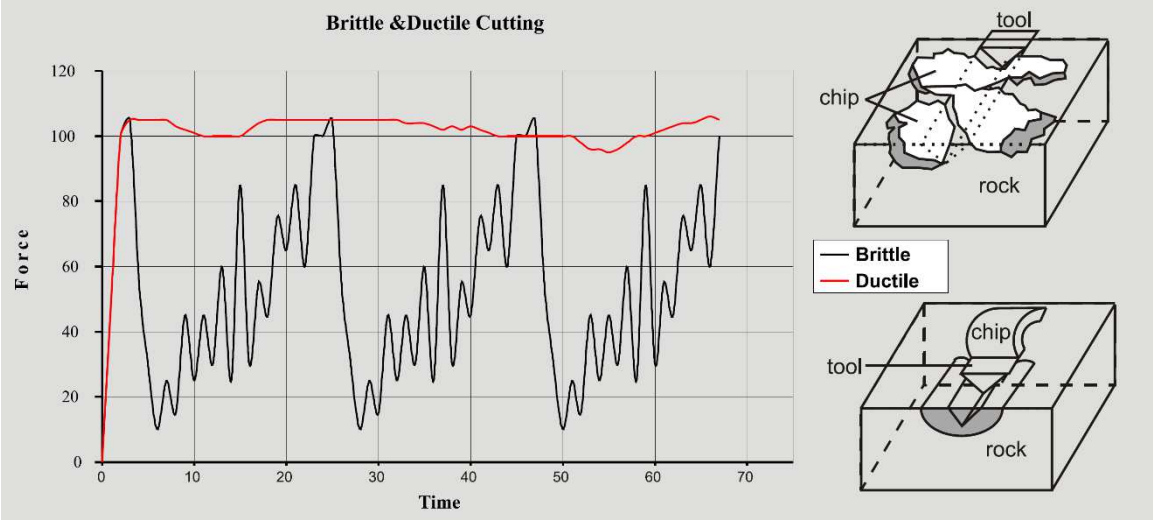

Figure 17 Ductile and Brittle Cutting extracted from Verhoef (1997)

Moreover, the way used to separate tensile failure, shear failure and a combination of both is to acknowledge that shear failure happens when the tensile strength σ_T is lower than the minimum horizontal principal stress σ_{min} with respect to the circle:

$$\frac{UCS}{BTS} = \frac{2}{\left(\frac{\sin\left(\frac{\alpha+\delta-\varphi}{2}\right)}{\cos\left(\frac{\alpha+\delta+\varphi}{2}\right)}-1\right)*\left(\frac{1-\sin(\varphi)}{\cos(\varphi)}\right)^2} \tag{3.6}$$

The change of formula for a shear failure is due to the need to correct the shear angle β of the flow type, Thus, the formula defining β becomes:

$$\beta = \frac{\pi}{2} - \frac{\alpha+\delta+\varphi+\pi/4}{2} \tag{3.7}$$

$$\frac{UCS}{BTS} = \frac{2}{\left(\frac{\sin\left(\frac{\alpha+\delta-\varphi-\pi/4}{2}\right)}{\cos\left(\frac{\alpha+\delta+\varphi-\pi/4}{2}\right)}-1\right)*\left(\frac{1-\sin(\varphi)}{\cos(\varphi)}\right)^2} \tag{3.8}$$

There are three possible modes of failure and three possible types of failure. Thus, in total, nine associations are possible and can be mapped on a diagram "Ratio -UCS/BTS" versus "Blade Angle α".

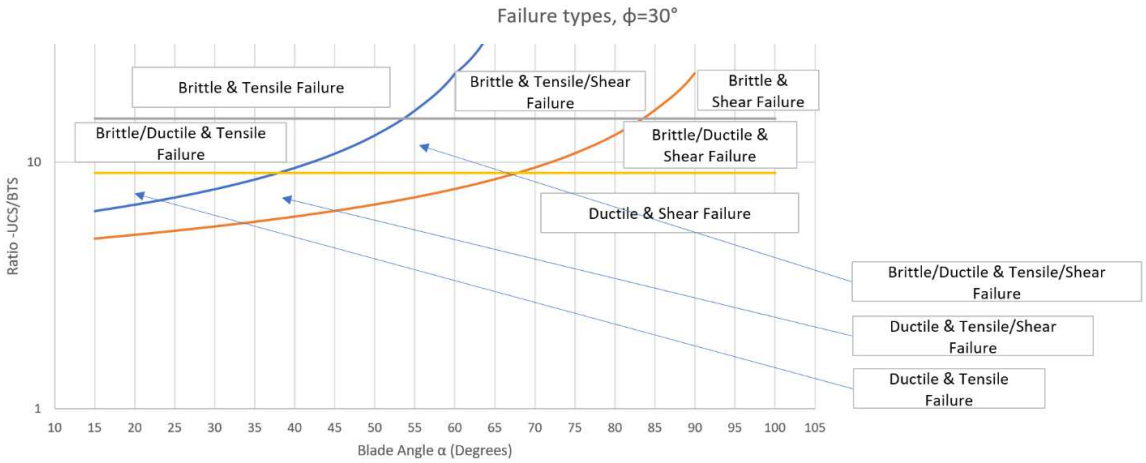

Figure 18 Map of the different Failure Mechanisms

3.1.3 The Models Corresponding to the Different Types/Modes

As it was said earlier, nine association of modes and types are possible. However, Miedema (2012) presented only six models. In addition, several models correspond to one

type of failure. Thus, some associations do not have any corresponding model. The models corresponding to each type of failure are summarized in the following scheme:

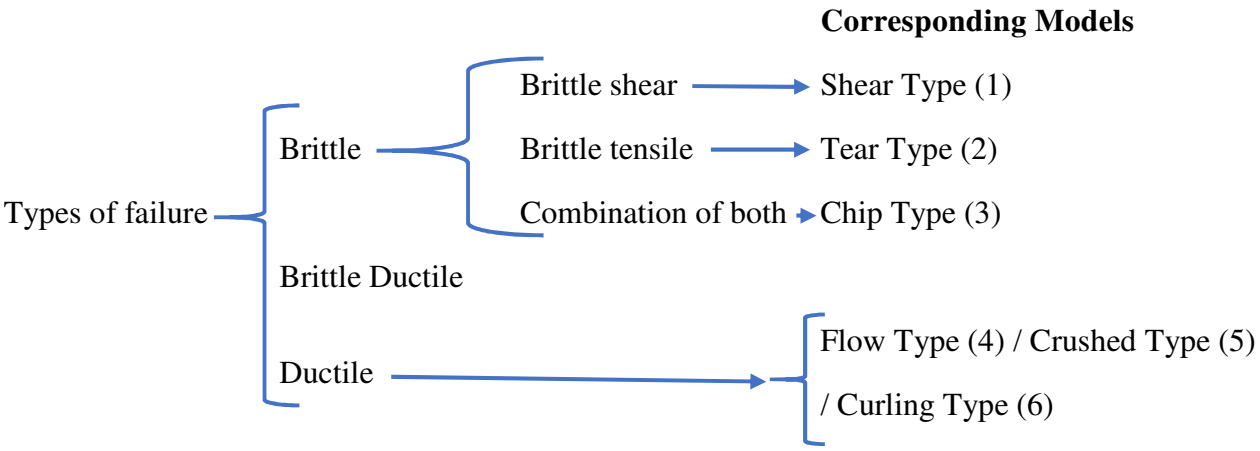

Figure 19 Schemes of Models and Types of Failure

The previous models are mapped on the following diagram "Ratio -UCS/BTS" versus "Blade Angle α" for the particular case of an internal failure angle of 30 degrees. As it was said earlier and in comparison with the previous map, the models do not cover the entire map.

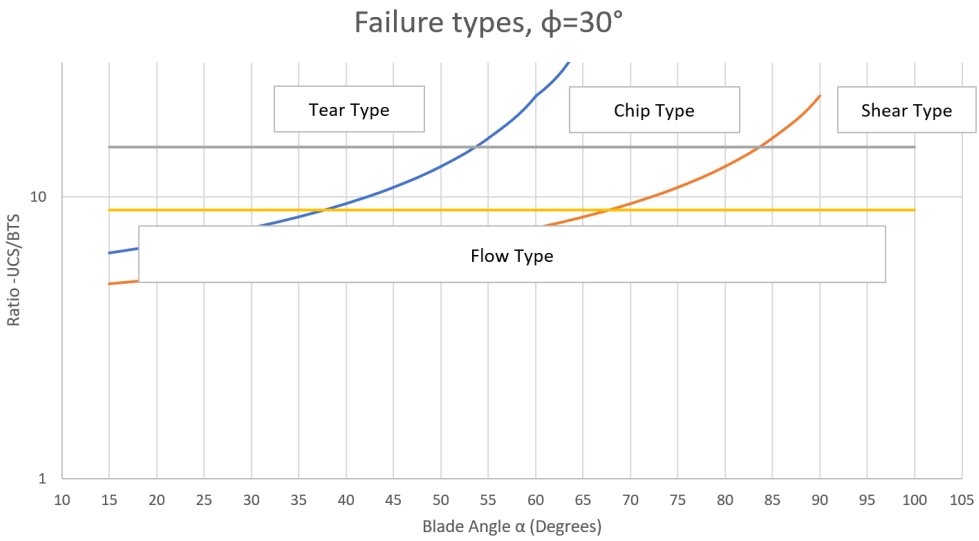

Figure 20 Map of the different Failure Models

In the next paragraph, the different models are presented and detailed and each model are illustrated by a scheme extracted from the work of Miedema (2012).

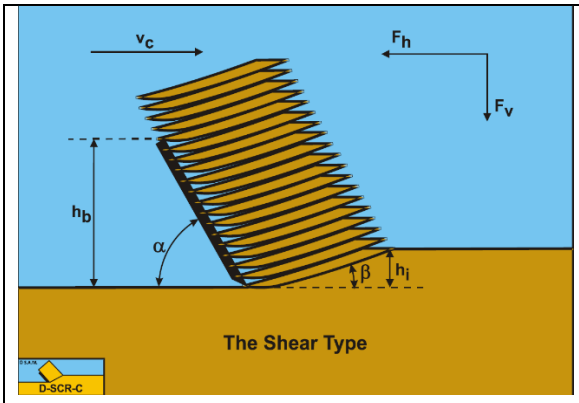

Figure 21 The Shear Type extracted from Miedema (2015)

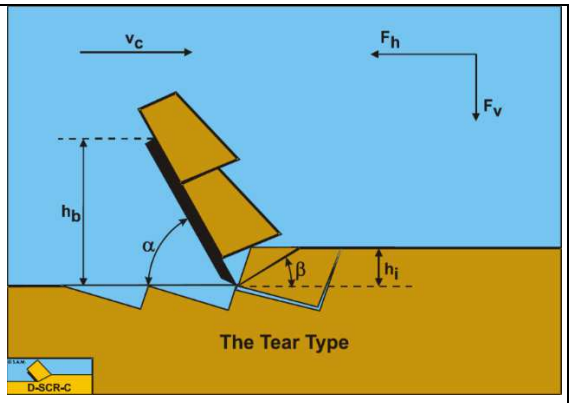

Figure 22 The Tear Type extracted from Miedema (2015)

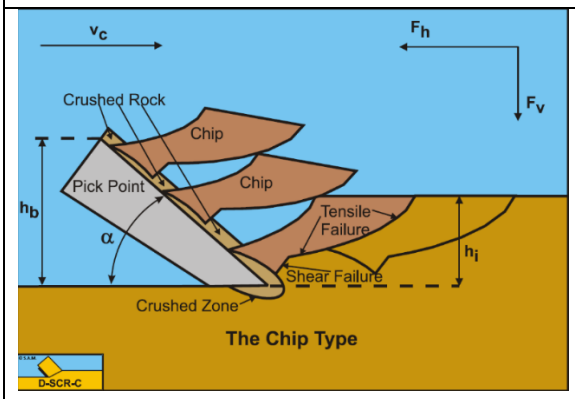

Figure 23 The Chip Type extracted from Miedema (2015)

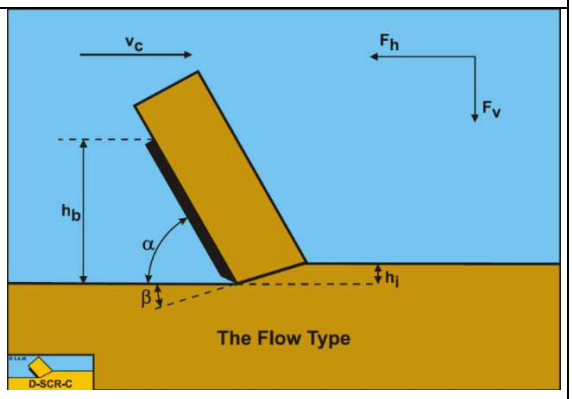

Figure 24 The Flow Type extracted from Miedema (2015)

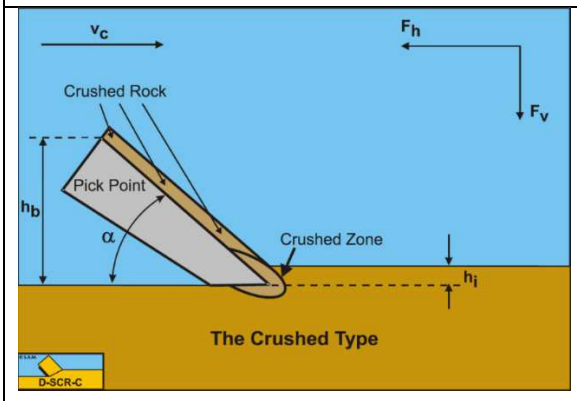

Figure 25 The Crushed Type extracted from Miedema (2015)

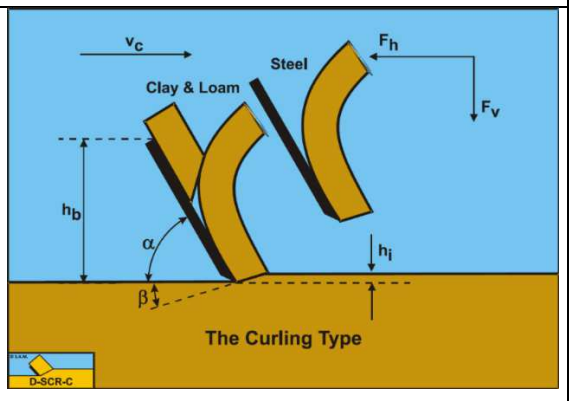

Figure 26 The Curling Type extracted from Miedema (2015)

1. **Shear Type:** The failure is 100% a shear failure. In fact, the normal stress in the shear plane and the unconfined tensile strength (UTS) or BTS are high. Usually, this failure type happens for large blade angles (α is high). It is a discontinues mechanism.
2. **Tear Type:** The failure is 100% tensile because the tensile strength is lower than the compressive strength. It is a discontinues mechanism.
3. **Chip Type:** The failure is a combination of the tensile failure and the shear failure.
4. **Flow Type:** It is a non-destructive continued plastic shear failure.
5. **Crushed Type:** The grain matrix is disintegrated. Thus, the failure is cataclistic based on shear. This type is very similar to the flow type.
6. **Curling Type:** The adhesive force is large in comparison with the normal force on the shear plane. This type is also called balling. This study will not take this one into account.

After defining these different model, the authors gave some relationships on the basis of the Merchant model at atmospheric conditions:

- For the **Flow Type** and **Crushed Type**:

$$MSE = \lambda_{HF} * c \tag{3.9}$$

$$\lambda_{HF} = \frac{2*\cos(\varphi)*\sin(\alpha+\delta)}{1+\cos(\alpha+\delta+\varphi)} \tag{3.10}$$

- For the **Shear Type**:

$$MSE = \lambda_{HT} * \sigma_T \tag{3.11}$$

$$\lambda_{HT} = \frac{2*\cos(\varphi)*\sin(\alpha+\delta)}{(1+\cos(\alpha+\delta+\varphi))*\left(\frac{\sin\left(\frac{\alpha+\delta-\varphi}{2}\right)}{\cos\left(\frac{\alpha+\delta+\varphi}{2}\right)}-1\right)*(\frac{1-\sin(\varphi)}{\cos(\varphi)})} \quad (3.12)$$

- For the **Tear Type** and **Chip Type**:

$$MSE = \lambda_{HT} * \sigma_T \quad (3.13)$$

$$\lambda_{HT} = \frac{2*\cos(\varphi)*\sin(\alpha+\delta)}{(\cos(a)+\cos(\alpha+\delta+\varphi))*\left(\frac{\sin\left(\frac{\alpha+\delta-\varphi-a}{2}\right)}{\cos\left(\frac{\alpha+\delta+\varphi-a}{2}\right)}-1\right)*(\frac{1-\sin(\varphi)}{\cos(\varphi)})} \quad (3.14)$$

3.2 A New Formulation for MSE

The apparent "strengthening" of the rock due to this mechanism is an inherent property of the rock. Thus, the new formulation presented, will be for the MSE_{min} instead of HMSE. In addition, what was introduced in the previous literature review concerns the atmospheric conditions. Obviously, the downhole conditions are not the same. The question is how to adapt these models from atmospheric to hydrostatic conditions.

To do so, the work of Detournay (2000) can be used. In fact, these authors showed that the strengthening effect of the bottom hole pressure (BHP) can be considered as an apparent additional cohesion. Thus, an apparent cohesion can be defined:

$$c_a = c + (p_h - p_o) * tan(\varphi) \quad (3.15)$$

where c is the cohesion, p_h is the bottom hole pressure, p_o is the pore pressure in the intact rock and φ is the internal friction angle.

Moreover, the experiences made by Rafatian (2009) showed that failure is brittle when the BHP is low (typically under 145 psi) and becomes ductile when the BHP become larger. Thus, most of the time when drilling the regime will be ductile and the approximation commonly made to compute MSE is correct. In addition, the formulation needs to be adapted in order to have the same symbols as in chapter 1:

$$MSE_{min} = \lambda_{HF} * c_a = \frac{2*cos(\varphi)*cos(\vartheta+\psi)}{1-sin(\vartheta+\psi+\varphi)}[c + (p_h - p_o) * tan(\varphi)] \quad (3.16)$$

$$\alpha = \frac{\pi}{4} - \frac{\vartheta+\psi+\varphi}{2} \quad (3.17)$$

$$\vartheta < \frac{\pi}{2} - (\varphi + \psi) \quad (3.18)$$

where ϑ is the rake angle, ψ is the contact friction angle and α is the shear failure plane inclination.

However, at atmospheric condition or at low BHP, this assumption is not correct and, because the failure is brittle. Thus, another formulation of MSE must be considered:

$$MSE_{min} = \lambda_{HT} * \sigma_T \quad (3.19)$$

With λ_{HT} corresponding to the type.

The assumption of this thesis is to apply the same idea of Detournay (2000) and to the other types of failures. Thus, at low BHP, this thesis assumes:

$$MSE_{min} = \lambda_{HT} * (\sigma_T + (p_h - p_b) * tan(\varphi)) \quad (3.20)$$

with λ_{HT} being equal to:

- For the **Shear Type**:

$$\lambda_{HT} = \frac{2*cos(\varphi)*cos(\vartheta+\psi)}{(1-sin(\vartheta+\psi+\varphi))*\left(\frac{\sin\left(\frac{\vartheta+\frac{\pi}{2}+\psi-\varphi}{2}\right)}{\cos\left(\frac{\vartheta+\frac{\pi}{2}+\psi+\varphi}{2}\right)}-1\right)*\left(\frac{1-\sin(\varphi)}{\cos(\varphi)}\right)} \quad (3.21)$$

- For the **Tear Type** and **Chip Type**:

$$\lambda_{HT} = \frac{2*cos(\varphi)*cos(\vartheta+\psi)}{(\cos(a)-sin(\vartheta+\psi+\varphi))*\left(\frac{\sin\left(\frac{\vartheta+\frac{\pi}{2}+\psi-\varphi-a}{2}\right)}{\cos\left(\frac{\vartheta+\frac{\pi}{2}+\psi+\varphi-a}{2}\right)}-1\right)*\left(\frac{1-\sin(\varphi)}{\cos(\varphi)}\right)} \quad (3.22)$$

This idea is supported by the different studies made by several authors that clearly shows that the curve of MSE is composed of two different parts. The first part is a straight

line corresponding to the brittle mode and which has a large slope. The second part is also a straight line which corresponds to the ductile mode and has a lower slope.

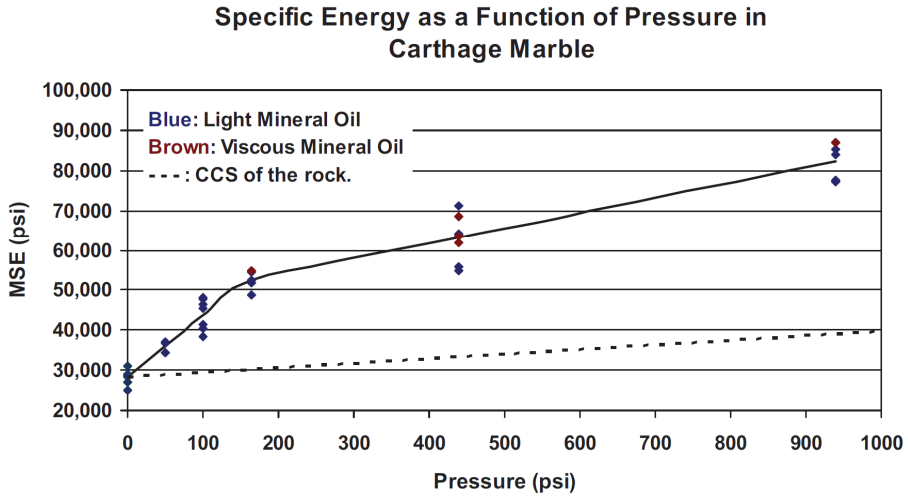

Figure 27 MSE vs. Confining Pressure for Carthage Marble in Light and Viscous Mineral Oil extracted from Rafatian (2009)

3.3 Examples Extracted from the Literature

Rafatian (2009) wrote a paper called "Experimental Study of MSE of a Single PDC Cutter Interacting with Rock Under Simulated Pressurized Conditions" In this paper he compared the evolution of the CCS and measured MSE in Carthage Marble when the pressure is increased. The graph he obtained is shown below.

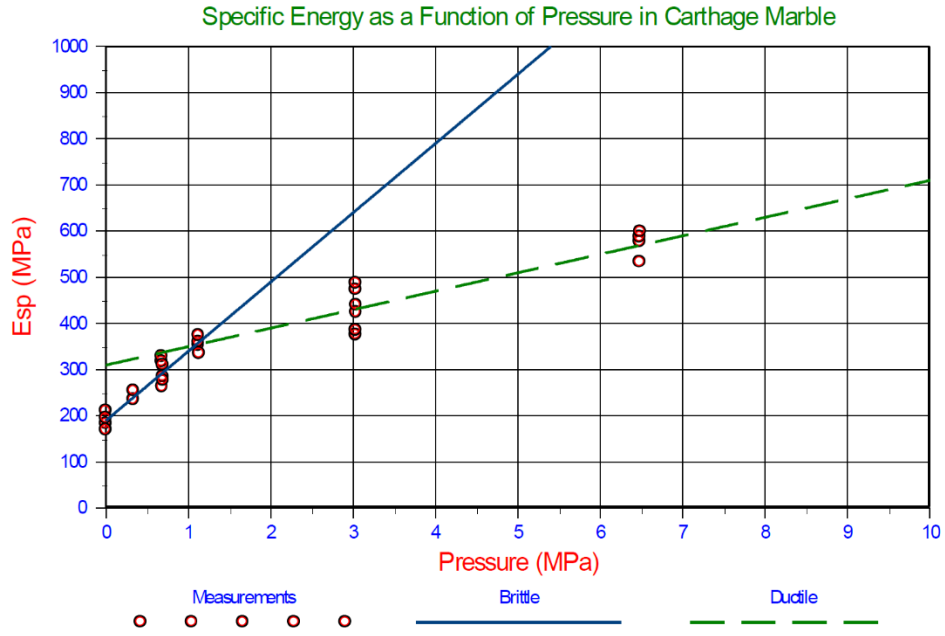

Figure 28 MSE vs. Confining Pressure for Carthage Marble in Light and Viscous Mineral Oil extracted from Miedema (2012)

The blade angle (α) is equal to 110°. Thus, ϑ is equal to 20°. The graph shows a change in slope: from 0 to 1.1 MPa the transition between brittle and ductile is going on and after 1.1 MPa the failure is completely ductile. Let us compare the slope with the theoretical values:

- Ductile part $slope_{experimental} \approx \frac{710-310}{10} \approx 40$,
  - $slope_{theoretical} \approx \frac{2*cos(\varphi)*cos(\vartheta+\psi)*tan(\varphi)}{(1-sin(\vartheta+\psi+\varphi))} \approx 40\ with\ \varphi = 35°\ and\ \psi = \frac{2}{3}*\varphi$.
- Brittle part $slope_{experimental} \approx \frac{490-190}{2} \approx 150$,
  - $slope_{theoretical} \approx \frac{2*cos(\varphi)*cos(\vartheta+\psi)*tan(\varphi)}{(\cos(a)-sin(\vartheta+\psi+\varphi))*\left(\frac{sin\left(\frac{\vartheta+\frac{\pi}{2}+\psi-\varphi-a}{2}\right)}{cos\left(\frac{\vartheta+\frac{\pi}{2}+\psi+\varphi-a}{2}\right)}-1\right)*\left(\frac{1-sin(\varphi)}{cos(\varphi)}\right)} \approx 157\ with\ a = 10.5°.$

In the same paper, Rafatian (2009) did the same experiment in Indiana Limestone.

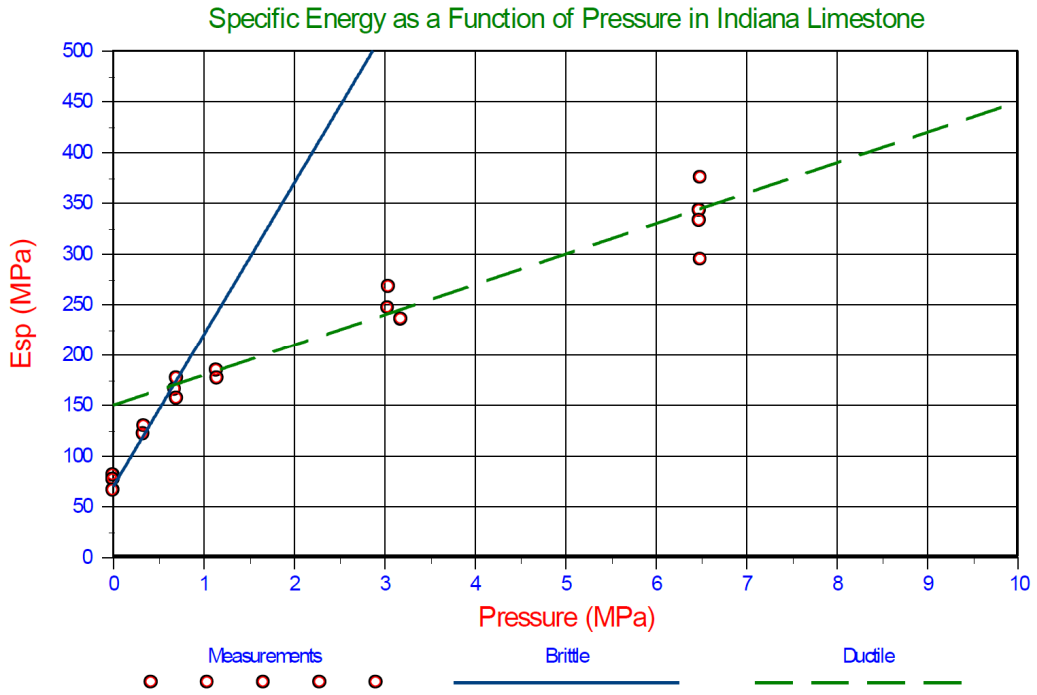

Figure 29 Confining Pressure for Indiana Limestone in Light Mineral Oil and Tap Water extracted from Miedema (2012)

The graph shows a change in slope: from 0 to 0.7 MPa the transition between brittle and ductile is going on and after 0.7 MPa the failure is completely ductile. Let's compare the slope with the theoretical values:

- Ductile part $slope_{experimental} \approx \frac{300-150}{5} \approx 30$,
  - $slope_{theoretical} \approx \frac{2*cos(\varphi)*cos(\vartheta+\psi)*tan(\varphi)}{(1-sin(\vartheta+\psi+\varphi))} \approx 30.5\ with\ \varphi = 34°\ and\ \psi = \frac{2}{3}*\varphi$.
- Brittle part $slope_{experimental} \approx \frac{490-190}{2} \approx 150$,
  - $slope_{theoretical} \approx \frac{2*cos(\varphi)*cos(\vartheta+\psi)*tan(\varphi)}{(\cos(a)-sin(\vartheta+\psi+\varphi))*\left(\frac{sin\left(\frac{\vartheta+\frac{\pi}{2}+\psi-\varphi-a}{2}\right)}{cos\left(\frac{\vartheta+\frac{\pi}{2}+\psi+\varphi-a}{2}\right)}-1\right)*\left(\frac{1-sin(\varphi)}{cos(\varphi)}\right)} \approx 142\ with\ a = 12°.$

Thus, using the results given by Miedema (2012), the idea of Detournay (1991) and the assumptions made, it is possible to match the theory with the experiments.

3.4 Application to Data

The model presented previously is going to be applied to the data provided by Marathon. To do so, some assumptions need to be done and a parameter study is going to be done. In the previous example the transition happens at 1.1 MPa (≃160 psi) and 0.7 MPa (≃131 psi). For the following example, the transition will be assumed to happen at 145 psi. Moreover, the angle a for the brittle part is set to 10.5° and 12°. For the following example, the angle a will be assumed to be equal to 11°.

Thus, this study is going to oppose the HMSE corrected with the change of failure mechanism and the HMSE not corrected. The formula is reminded below:

$$EFF_M = \frac{MSE_{min}}{HMSE} \tag{3.23}$$

Where the formulation of MSE_{min} shift from brittle (Eq. 3.24) to ductile (Eq. 3.25) when the differential pressure increases above 145 psi.

$$MSE_{min} = UCS + \lambda_{HT} * (p_h - p_b) * tan(\varphi) \tag{3.24}$$

$$MSE_{min} = MSE_{min}(145) + \lambda_{HF} * (p_h - p_b - 145) * tan(\varphi) \tag{3.25}$$

The following graph is showing two lines. The red line is the efficiency not corrected for the change of failure mechanism. The blue line is the efficiency corrected for this change. As the reader can see, the two lines can be distinguished at the beginning and as the separation disappears as the depth increases.

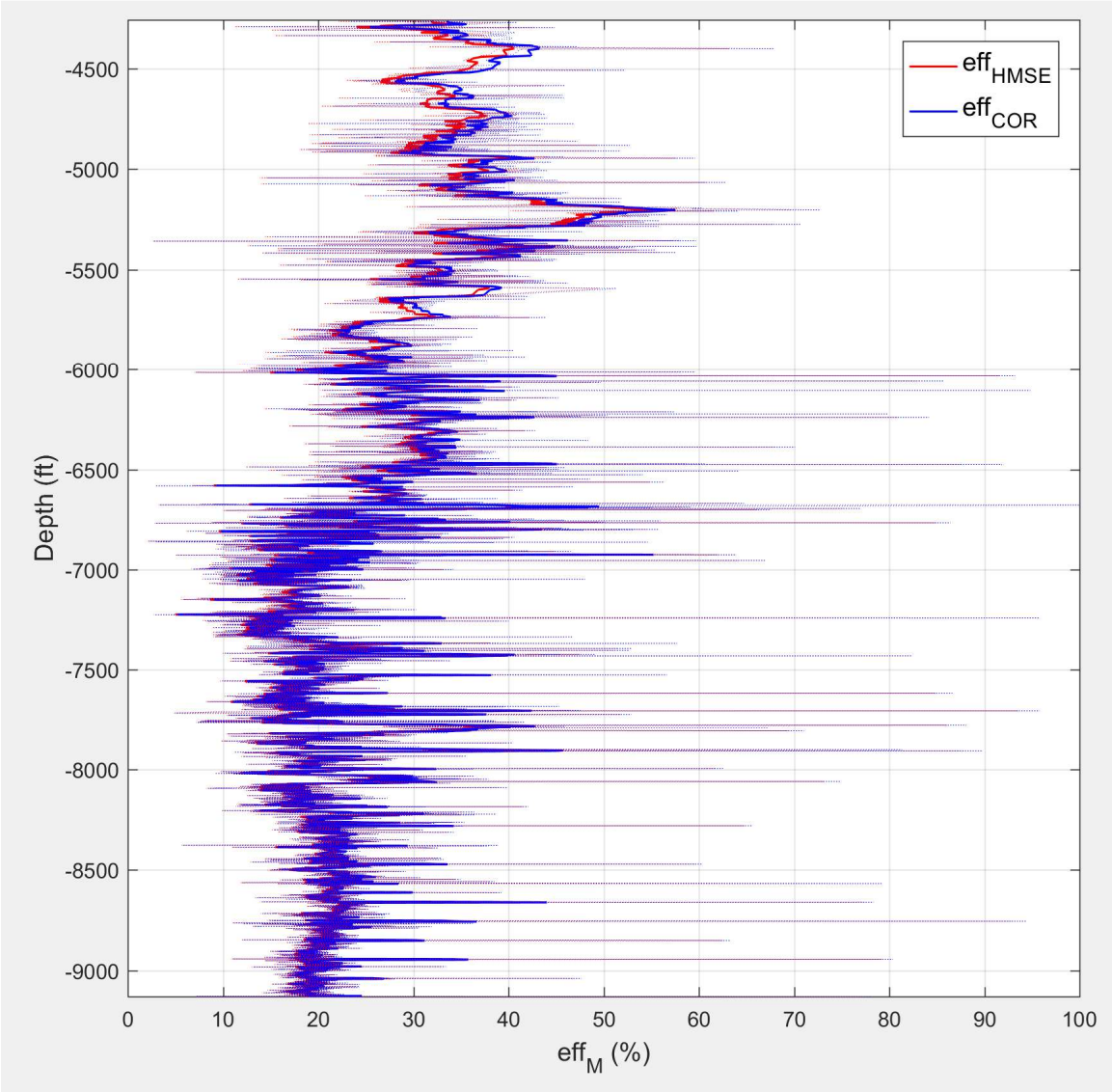

Figure 30 Influence of Change in Failure Mechanism

The two following tables are here to help quantify the importance of this phenomenon depending on the nature on the stone. The first table shows the average difference between the EFF_M calculated considering the change in failure mechanism and the EFF_M without taking into account this change.

Rock Type	Eff_M (MSE) (%)	Eff_M (Corrected) (%)	Average Difference (%)
Sandstone	21.87	22.46	0.59
Limestone	22.26	22.68	0.41
Shale	23.85	24.56	0.71

Table 14 Influence of Change in Failure Mechanism per Rock Type

As one can see there is no relationship clear relationship between the nature of the rock and the average difference. Globally the average difference created when considering the change in failure mechanism is around 0.57%. Thus, in this particular case, the difference can be considered negligible. However, as it will be showed in the parameter studies the difference can easily increase to non-negligible amounts.

Formation Name	Eff_M (MSE) (%)	Eff_M (Corrected) (%)	Average Difference (%)
Greenhorn	32.93	34.92	1.99
Newcastle	31.69	33.58	1.89
Dakota	34.11	35.90	1.80
Swift	39.48	41.11	1.63
Rierdon	28.23	29.29	1.06
Piper	27.95	28.62	0.67
Spearfish	31.19	31.98	0.79
Pine Salt	24.10	24.62	0.52
Broom Creek	18.20	18.75	0.55
Tyler	17.95	18.47	0.52
Kibbey Lime	18.29	18.60	0.31
Charles	20.73	21.10	0.37
Ratcliffe	22.01	22.49	0.48
Base Last Salt	18.51	18.85	0.34
Mission Canyon	21.74	22.02	0.29
Lodgepole	19.53	19.79	0.26

Table 15 Influence of Porosity on Shear Dilatancy per Formation

As one can see, the difference between the EFF_M corrected and the EFF_M is decreasing as the depth increases. This fact can be explained by the fact that the difference between the BHP and the pore pressure decreases as the depth increases.

3.5 Parameter Study

3.5.1 Angle *a*

The angle *a* was found to be equal to 10.5° and 12° in the examples presented above. In the following parameter study, a is going to take five values: 5°, 10°, 15°, 20°, and 25°.

Rock Type	Average Difference (%)				
	a=5°	**a=10°**	**a=15°**	**a=20°**	**a=25°**
Sandstone	0.05	0.48	1.26	2.97	7.96
Limestone	0.04	0.33	0.88	2.07	5.54
Shale	0.06	0.57	1.51	3.56	9.45

Table 16 Influence of Angle a on Change in Failure Mechanism

As one can see the difference increases when the angle *a* increases.

3.5.2 Pressure of the Change in Failure Mechanism

The pressure at which the change of failure mechanism occurs at 130 psi and 161 psi in the examples presented above. In the following parameter study, this pressure varies from 0 psi to 400 psi with 100 psi increments.

Rock Type	Average Difference (%)				
	0 psi	**100 psi**	**200 psi**	**300 psi**	**400 psi**
Sandstone	0.00	0.41	0.82	1.23	1.64
Limestone	0.00	0.28	0.57	0.85	1.14
Shale	0.00	0.49	0.98	1.47	1.96

Table 17 Influence of the Pressure Change on Change in Failure Mechanism

As the reader can see, the average difference increases when the transition increases. This phenomenon can be very easily explained by the fact that the slope of the brittle mode is larger than the slope of the ductile mode.

3.6 Conclusion

The impact of failure mechanism has been studied and quantified and a way to account for it in the formulation of MSE and particularly in the formulation of MSE_{min}. As the reader might have noticed, two information are needed to apply this theory: the angle a and the transition pressure. These two physical values can be obtained through core experiment as showed in the examples.

The parameter study showed that the transition pressure does not have a very strong impact on the difference. However, the angle *a* has a real impact on the difference between the efficiency computed with and without the change in failure mechanism. To illustrate this idea, the following graph shows these two efficiencies for an angle *a* equal to 25 degrees. Moreover, it can be acknowledged that theoretically the angle *a* can take values between 0 and 45 degrees, but values over 25 degrees or so create efficiencies over 100% at the top of the section.

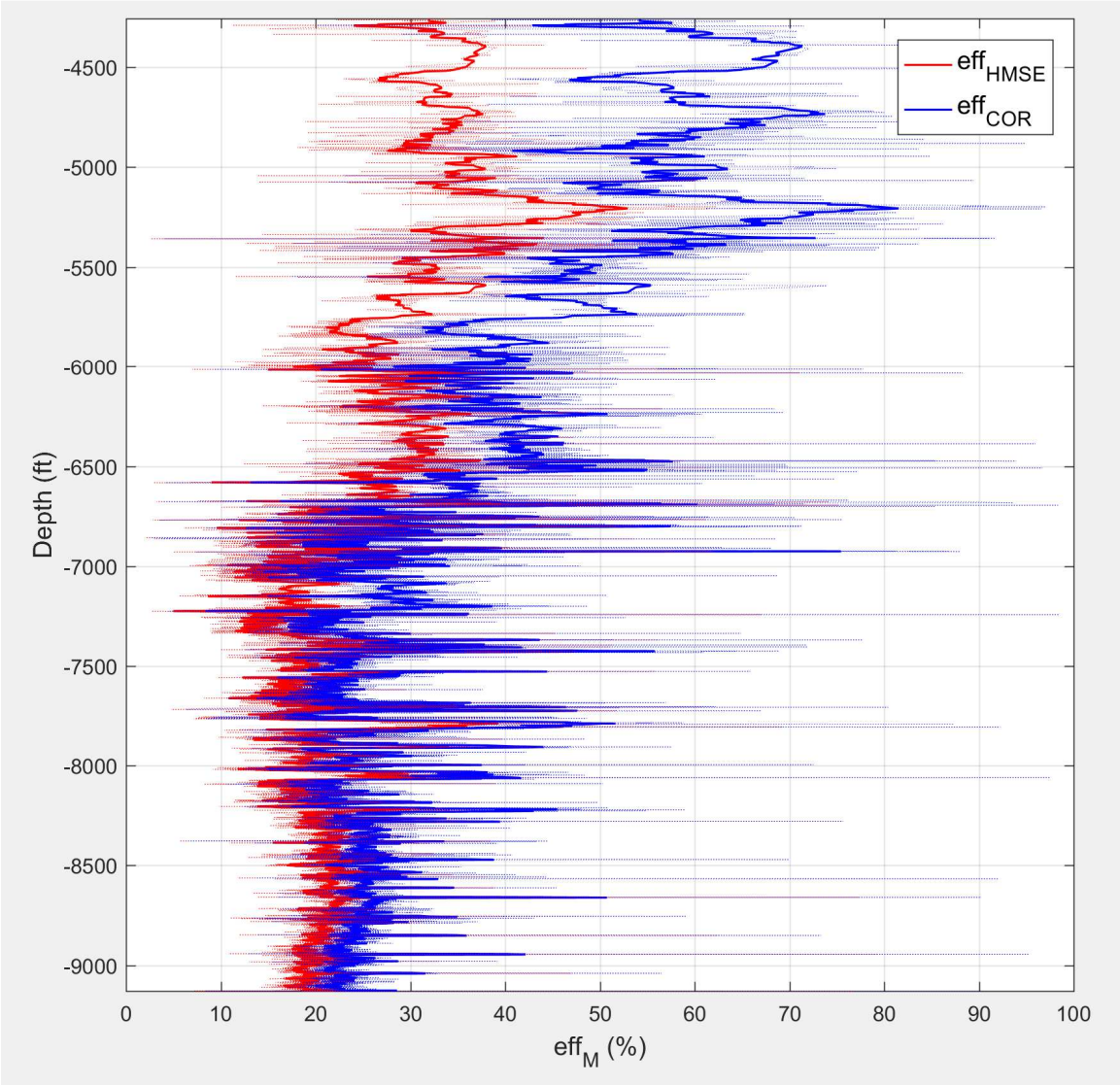

Figure 31 Influence of Change in Failure Mechanism with α=25 deg

Chapter 4: The Program

4.1 Input

4.1.1 Choice of the Phenomena to Consider

The first question asked to the user is what phenomenon he wants to consider into the calculation of Mechanical Specific Energy (MSE). To do so a dialog box appears with two questions:

- "Do you want to consider the shear dilatancy? [0/1]". If the answer is "0", it means "No" and if the answer is "1", it means "Yes".
- "Do you want to consider change of failure mechanism? [0/1]". If the answer is "0", it means "No" and if the answer is "1", it means "Yes".

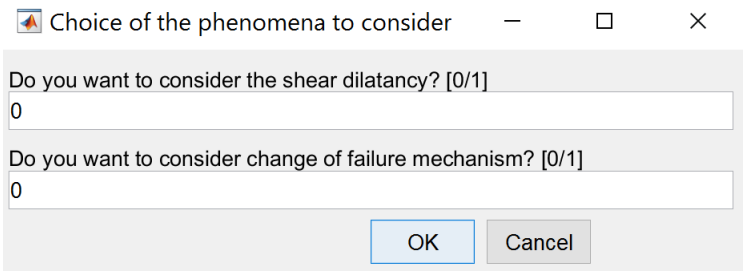

Figure 32 Dialog Box: Choice of the Phenomena to Consider

4.1.2 Data Extraction

The source file is an excel sheet containing the different physical values measured at the surface or downhole by an instrument the COP. The important physical values to be extracted are:

- The depth in feet
- The differential pressure (measured downhole) in psi

- The rotational speed (measured downhole) in rotations by minute.
- The Hydraulic Mechanical Specific Energy (HMSE measured downhole) in psi
- The formation name
- The formation type
- The Unconfined Compressive Strength (UCS) in psi

The rotational speed, the formation name and the formation type are only used to compute the effect of shear dilatancy. Thus, when the variable *shear_dilatancy* is set to 0 or in other words the user does not want to consider shear dilatancy, these data will not be extracted.

4.1.3 Formation Assumptions

The assumptions which need to be made on the porosity (k), permeability (Φ) and internal friction angle (φ). The choice made was to give only one value for porosity and permeability for each formation type. Moreover, only one value is given for the internal friction angle for the all the section drilled.

The permeability and porosity will be needed to compute the shear dilatancy. Whereas the internal friction angle is used to calculate the *m* which is the multiplication factor used to calculate the minimum Mechanical Specific Energy (MSE_{min}) and the strengthening due to shear dilatancy.

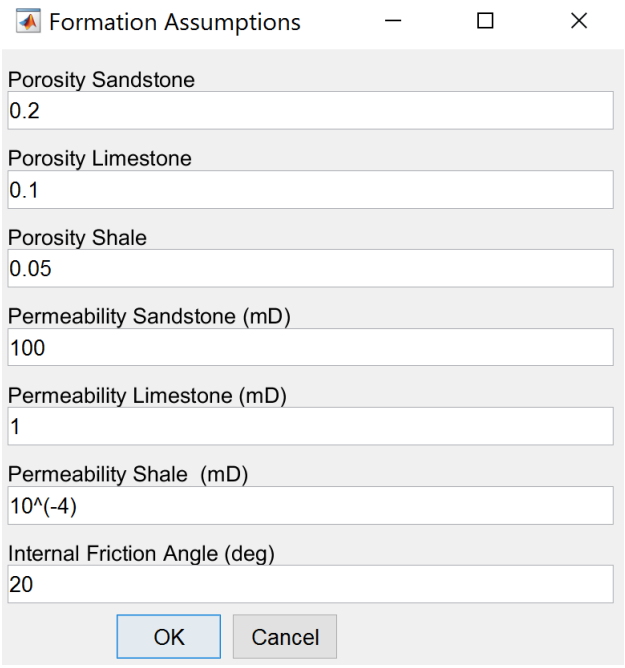

Figure 33 Dialog Box: Formation Assumptions

From the internal friction angle, the Mohr Coulomb friction coefficient is going to be deduced. In addition, the porosity and permeability are only used to compute the effect of shear dilatancy. Thus, if the *shear_dilatancy* variable is set to 0, only the internal friction angle will be asked.

4.1.4 Fluid Assumptions

Some assumptions need to be done on fluid properties. These properties are going to be used to compute the effect of shear dilatancy. The fluid compressibility (C_f) and the viscosity (μ) are going to be set to one value for the whole section drilled.

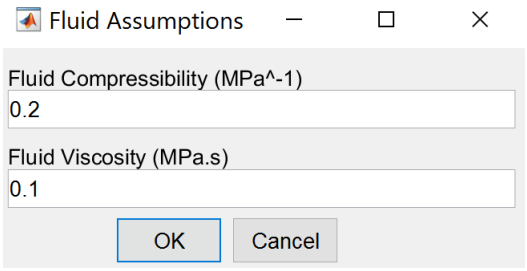

Figure 34 Dialog Box: Fluid Assumptions

Since these properties are only useful to quantify the strengthening due to shear dilatancy if the user set the *shear_dilatancy* variable to 0, the fluid assumptions will not be asked.

4.1.5 Bit Assumptions

One value will be given for each the siderake angle (β), the backrake angle (θ) and the depth of cut (δ) for the section drilled. The assumptions made for these three values will be necessarily wrong since each cutter of the bit could have a different depth of cut, a different siderake angle and different backrake angle. From these values, some other physical values will be deduced:

- The lateral angle of failure (α_s)
- The normal angle of failure (α_n)
- The lateral angle of friction (ψ_s)
- The normal angle of friction (ψ_n)

These are going to be used to compute the *m* factor and thus have a huge impact on the final results. Moreover, the user can choose between three options: calculating *m* in 1D, 2D or 3D:

- $m_{1D} = \frac{2*\sin(FA)}{1-\sin(FA)}$
- $m_{2D} = \frac{2*cos(\varphi)*cos(\vartheta+\psi)}{1-sin(\vartheta+\psi+\varphi)}$
- $m_{3D} = \frac{cos(\alpha_S)*(cos(\theta+\psi_n)+tan(\beta)*tan(\psi_s))}{sin(\alpha_n)*(cos(\alpha_n+\theta+\psi_n)-k*cos(\alpha_S)*sin(\alpha_n+\theta+\psi_n))}$

The strengthening due to shear dilatancy is going to be computed with m_{3D} since its formulation was developed in this thesis. The effect of change in failure mechanism creates a new formulation for MSE_{min} this formulation will use m_{2D} necessarily.

In addition, some information is also needed on the position of the cutters to compute the velocity of the cutters. The interesting values can be found in the vendor information and are:

- The bit diameter
- The number of zones the reader wants to define
- The number of cutters inside each zone

These values are used to compute the strengthening due to shear dilatancy for each radius and then this effect is average using the number of cutters in each zone. As a reminder, in the example done in chapter 2, five zones were defined.

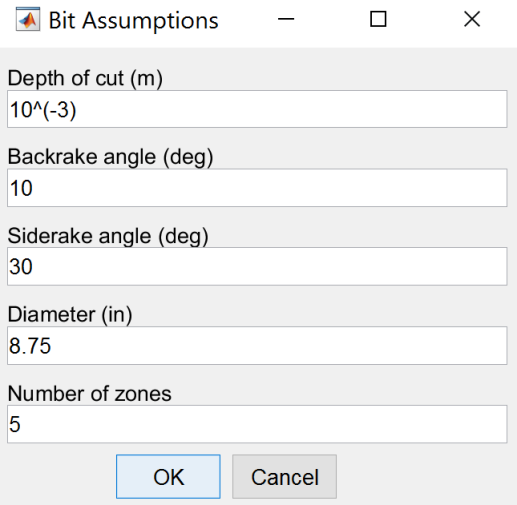

Figure 35 Dialog Box: Bit Assumptions

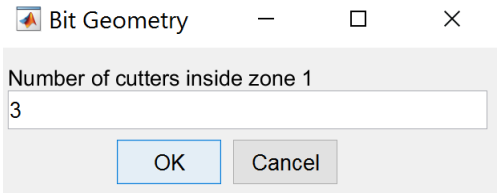

Figure 36 Dialog Box: Bit Geometry

4.2 Output

4.2.1 Graph

The first output is a graph of the depth versus the efficiency in percent. This graph contains two curves representing the efficiency before and after correction (respectively EFF_{HMSE} and EFF_{COR}).

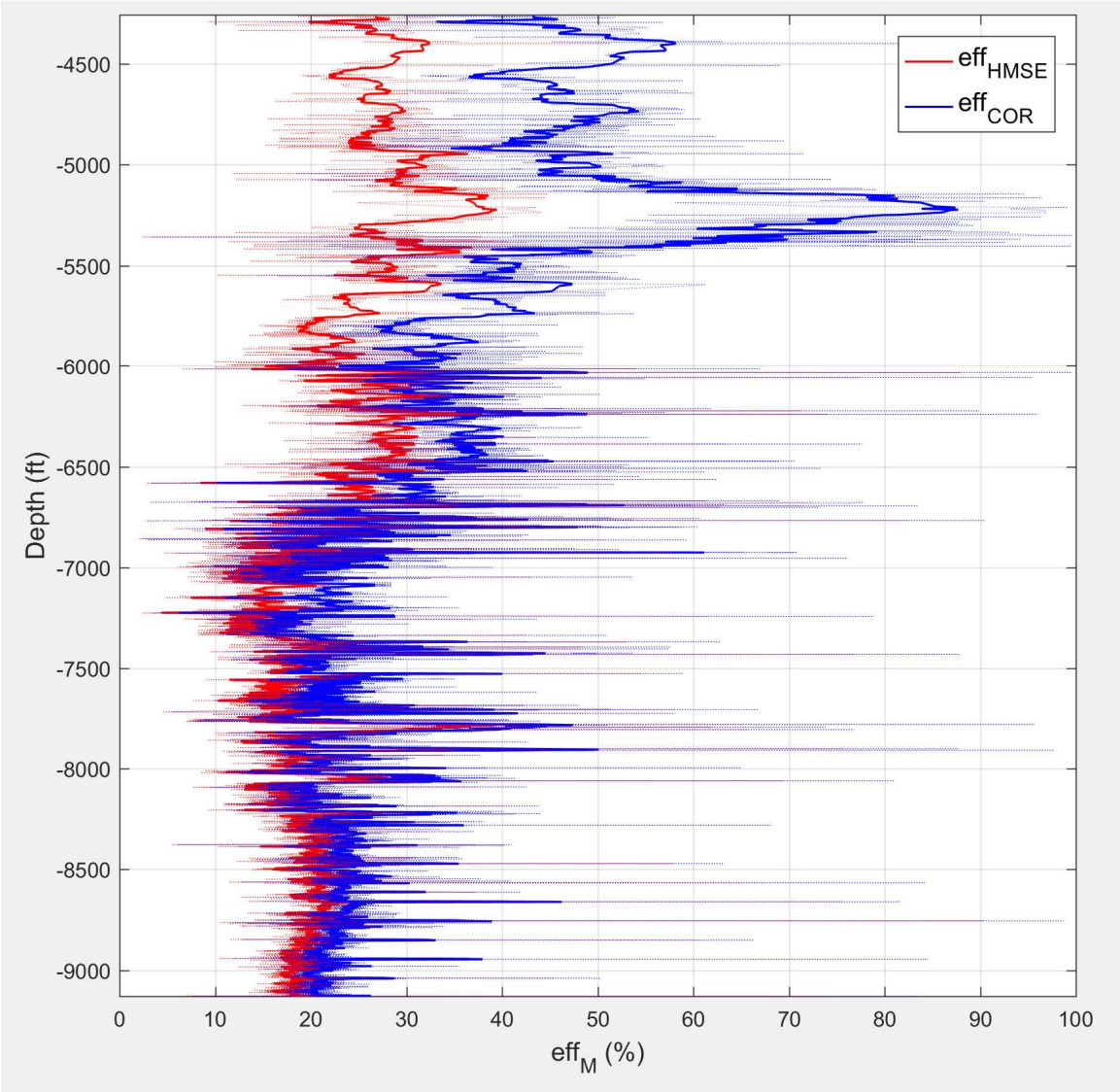

Figure 37 Output: Graph

4.2.2 Excel Sheet

The second output is an Excel sheet called "results.xls". This sheet contains three tables. The first gathers the average EFF_{HMSE}, the average EFF_{COR} and the average difference between the two for each rock type. The third one gathers the same information but averaged for each formation. Finally, the second one, shows the number of data points

not considered and what this number represent in comparison to the number of data points provided (in percent). As a reminder, all the points with an efficiency below 0% or above 100% were suppressed.

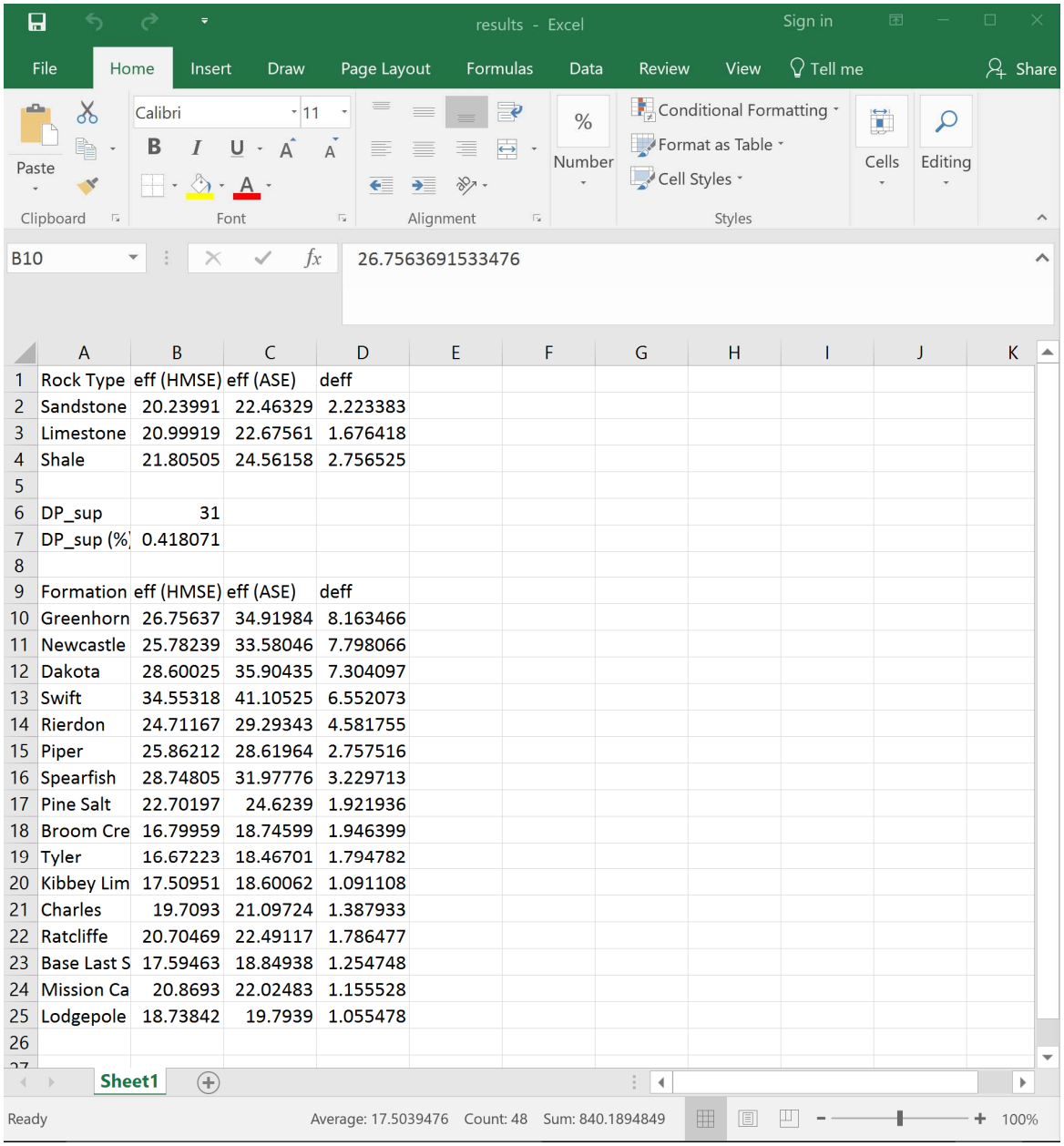

	A	B	C	D
1	Rock Type	eff (HMSE)	eff (ASE)	deff
2	Sandstone	20.23991	22.46329	2.223383
3	Limestone	20.99919	22.67561	1.676418
4	Shale	21.80505	24.56158	2.756525
5				
6	DP_sup	31		
7	DP_sup (%)	0.418071		
8				
9	Formation	eff (HMSE)	eff (ASE)	deff
10	Greenhorn	26.75637	34.91984	8.163466
11	Newcastle	25.78239	33.58046	7.798066
12	Dakota	28.60025	35.90435	7.304097
13	Swift	34.55318	41.10525	6.552073
14	Rierdon	24.71167	29.29343	4.581755
15	Piper	25.86212	28.61964	2.757516
16	Spearfish	28.74805	31.97776	3.229713
17	Pine Salt	22.70197	24.6239	1.921936
18	Broom Cre	16.79959	18.74599	1.946399
19	Tyler	16.67223	18.46701	1.794782
20	Kibbey Lim	17.50951	18.60062	1.091108
21	Charles	19.7093	21.09724	1.387933
22	Ratcliffe	20.70469	22.49117	1.786477
23	Base Last S	17.59463	18.84938	1.254748
24	Mission Ca	20.8693	22.02483	1.155528
25	Lodgepole	18.73842	19.7939	1.055478
26				

Figure 38 Output: Excel Sheet

Chapter 5: Conclusion

5.1 Shear Dilatancy

5.1.1 Present Work

When the cutter goes forward inside the rocks, it provokes the rock to shear which creates dilatancy. This phenomenon gives this name to the phenomenon of shear dilatancy. The issue is that this dilatation creates a change in porosity, then a change in pore pressure which will finally increases the differential pressure. Since MSE is proportional to the differential pressure, this phenomenon will increase MSE, in other words, shear dilatancy creates a strengthening of the rock.

Adapting existing studies and making the appropriate assumptions, a new formulation was derived for the mechanical specific energy and, in particular, for the HMSE. In fact, the choice was made to consider shear dilatancy as a phenomenon which is controlled by drilling parameters instead of both rock properties and differential pressure between BHP and P_o. This idea is due to the fact that the strengthening effect is controlled (among other things) by the velocity of the cutter which can be directly controlled by the rotational speed of the bit.

In order to be able to distinguish HMSE from this physical value taking into account shear dilatancy, the adapted specific energy (ASE) was created. This value consists in the work done to destroy the rock, i.e. HMSE, minus the strengthening effect due to shear dilatancy.

The formulation of this strengthening effect can take three forms corresponding to the three regimes described in the literature. The first regime is the “high speed regime”, In this case cavitation occurs and the MSE will depend only on the bottom hole pressure

instead of the differential pressure. It is when the strengthening effect is the largest. The second is the "transient regime". In this regime shear dilatancy plays a lower role since full cavitation does not occur. Finally, the third possible regime is the "low speed regime". In this case, the rock fails in a drained manner and thus the pressure in the sheared rock is the same as the pressure in the intact rock. In this last case, there is no strengthening effect.

After making the right assumptions, this new formulation of MSE was used on the data Marathon provided. Then a parameter study was made which showed that the main parameter controlling this phenomenon is the shear dilatancy and thus, in the rocks with very low permeability like shales, cavitation is very likely to happens and the strengthening effect will be very important creating an average difference between EFF_{HMSE} and EFF_{ASE} higher than 23% in certain cases.

5.1.2 Future Work

Three improvements could be made on this topic:

- First the function $g(\vartheta;\lambda)$ should be calculated in an exact way instead of using an Hermite element.
- Then the theory of Detournay (1991) and, in particular, the same function $g(\vartheta;\lambda)$ should be adapted to 3D. In fact, this function only depends on the backrake angle instead of depending on the backrake and siderake angles.
- A lot of assumptions have been made on the porosity/permeability/internal friction angle of the rock which could be suppressed using core experiments. Thus, a set of data with more information could strengthen a lot this theory.

5.2 Change of Failure Mechanisms

5.2.1 Present Work

The observation was made by several authors that when increasing the differential pressure (i.e. the difference between the mud pressure and the pore pressure) the failure mechanism changes from brittle to ductile. Practically, this change can easily be noticed by observing the cutting shape. The brittle mode creates chip like cuttings whereas the ductile mode creates ribbon like cuttings. Each of these shapes correspond to wo entirely different failure mechanisms. According to Block (2009), the ductile mode happens "when the rock is unable to carry load after reaching its peak strength." Whereas the ductile mode happens "when the rock continues to carry load after failure."

The work of several authors was compiled and making appropriate assumptions a new formulation for MSE and, in particular, for the MSE_{min}. In fact, change in failure mechanism phenomenon which only depends on rock properties and differential pressure between BHP and P_o, Thus, it changes the calculation of MSE_{min} instead of HMSE.

This new formulation of MSE_{min} has been validated on two example extracted from the work of Rafatian (2009). Once this validation was done, the newly developed theory was applied to the data provided by Marathon creating a very low average difference (less than 1%). However, the parameter study showed that this different is highly dependent on the parameters chosen and could lead to differences as high as 9.45%.

5.2.2 Future Work

The main drawback of this theory is the lack of data. Only two information are needed to implement this theory: The angle *a* and the transition pressure. These two physical values could be easily obtained using core experiments. Thus, a more complete set of data could be very useful to develop this theory.

5.3 The Program

5.3.1 Present Work

A MATLAB code has been developed to allow a user to consider shear dilatancy and change in failure mechanism while calculating the efficiency. To do so, several dialog boxes open asking for different parameters on the formation properties, the fluid properties and the bit properties. The dialog boxes are adapted to the phenomenon considered. For example, since the fluid nature only impacts the strengthening due to shear dilatancy, in case the user chose to consider only the effect of change in failure mechanism, this particular box will not appear.

The output of this program are:

- A graph showing two curves corresponding to the efficiency before and after taking into account the phenomenon.
- An Excel sheet containing the efficiencies (before/after) and difference between those two averaged for the rock types and the formations

5.3.1 Future Work

Several improvements could be made to this program:

- First some parameters are set for the whole section drilled. A good improvement would be to give the user the opportunity to make these parameters vary in function of the rock type or of the formation drilled.
- In addition to the present graph some other could be created as HMSE vs ASE or CCS versus MSE_{min}.

5.4 Conclusion

This thesis has proposed two new formulations for both considering shear dilatancy and change in failure mechanism into the calculation of mechanical specific energy and mechanical efficiency. It has been shown that the importance of these phenomena highly depend on the drilling parameters and rock properties. Thus, in the case of the Marathon data, several assumptions have been made. Further work must be done with more data, including core experiments and well logs to have a better appreciation of the importance of these phenomena while drilling.

References

- Armenta, M. 2008. Identifying Inefficient Drilling Conditions Using Drilling-Specific Energy. Paper SPE 116667 presented at the 2008 SPE Annual Technical Conference and Exhibition, Denver, Colorado, USA, September 21-24.
- Black, A.D. and al. 2008. Optimization of Deep-Drilling Performance With Improvements in Drill-Bit and Drilling Fluid Design. Paper SPE-112731-MS presented at the IADC/SPE Drilling Conference, Orlando, Florida, USA, March 4-6
- Block, G. and Jin, H. 2009. Role of Failure Mode on Rock Cutting Dynamics. Paper SPE-124870-MS presented at the SPE Annual Technical Conference and Exhibition, New Orleans, Louisiana, October 4-7
- Caicedo, H.U. and al. 2005. Unique ROP Predictor Using Bit-specific Coefficient of Sliding Friction and Mechanical Efficiency as a Function of Confined Compressive Strength Impacts Drilling Performance. Paper SPE-92576-MS presented at the SPE/IADC Drilling Conference, Amsterdam, The Netherlands, February 23-24.
- Cook, J.M. and al. 1991. Effects of Strain Rate and Confining Pressure on the Deformation and Failure of Shale. Paper SPE-19944-PA. SPE Drilling Engineering Vol. 6
- Detournay, E. and Atkinson, C. 1991. Influence of Pore Pressure on the Drilling Response of PDC Bits. Paper ARMA-91-539 presented at the 32nd U.S. Symposium on Rock Mechanics (USRMS), Norman Oklahoma, July 10-12
- Detournay, E. and Atkinson, C. 2000. Influence of Pore Pressure on the Drilling Response in Low-permeability Shear-dilatant Rocks. International Journal of Rock Mechanics and Mining Sciences, Vol. 37, Issue 7, 1091-1101

- Gehring, K. 1987. Rock Testing Procedures at VA's Geotechnical Laboratory in Zeltweg. Zeltweg, Austria, Voest Alphine, International Report TZU 48
- Gray-Stephens, D. and al. 1994. Influence of Pore Pressure on Drilling Response in Hard Shales. Paper SPE-23414-PA. SPE Drilling & Completion, Vol. 9
- Ledgerwood III, L.W. 2007. PFC Modeling of Rock Cutting Under High Pressure Conditions. Paper ARMA-07-063 presented at the 1st Canada – U.S. Rock Mechanics Symposium, Vancouver, Canada, May 27-31
- Miedema, S.A. and Zijsling, D. 2012. Hyperbaric Rock Cutting. Paper presented at the ASME 2012 31st International Conference on Ocean, Offshore and Artic Engineering, Rio de Janeiro, Brazil, July 1-6
- Miedema, S.A. 2015. The Delft Sand, Clay & Rock Cutting Model. 2nd edition, 2015, version: Wednesday, January 27, 2017.
- Mohan, K. and al 2009. Tracking Drilling Efficiency Using Hydro-Mechanical Specific Energy. Paper SPE-119421-MS presented at the 2009 SPE/IADC Drilling Conference and Exhibition, Amsterdam, The Netherlands, March 17-19.
- Pessier, R.C. and Fear, M.J. 1992. Quantifying Common Drilling Problems with Mechanical Specific Energy and Bit-Specific Coefficient of Sliding Friction. Paper SPE 24584 presented at the 67th Annual Technical Conference and Exhibition, Washington, DC, October 4-7.
- Rabia, H. 1989. Rig Hydraulics. Entrac Software, England.
- Rafatian, N. and al. 2009. Experimental Study of MSE of a Single PDC Cutter Under Simulated Pressurized Conditions. Paper SPE-119302-MS presented at the SPE/IADC Drilling conference and Exhibition, Amsterdam, The Netherlands, March 17-19.
- Simon, R. 1963. Energy Balance in Rock Drilling. Paper SPE-499-PA Society of Petroleum Engineers Journal Vol. 3

- Teale, R. 1965. The Concept of Specific Energy in Rock Drilling. Intl. J. Rock Mech. Mining Sci., Vol. 2, 57-73.
- Verhoef, P. 1997. Wear of Rock Cutting Tools: Implications for Site Investigation of Rock Dredging Projects. Delft, The Netherlands: Balkema Rotterdam
- Warren, T.M. 1987. Penetration Rate Performance of Roller Cone Bits. Paper SPE-13259-PA SPE Drilling Engineering Vol. 2
- Zijsling, D.H. 1987. Single Cutter Testing – A Key for PDC Bit Development. Paper SPE-16529-MS. Offshore Europe, Aberdeen, United Kingdom, September 8-11